Cell Reports

Article

Culture conditions of mouse ESCs impact the tumor appearance *in vivo*

Graphical abstract

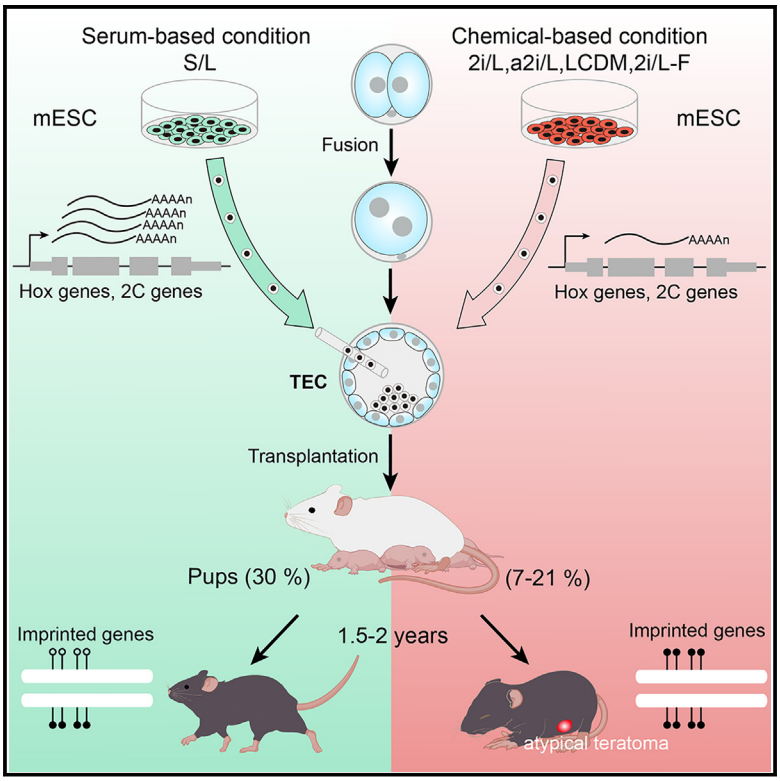

Highlights

- Culture conditions affect ESC pluripotency and long-term differentiation potential
- Conventional serum/Lif ESC cultures produce healthy pups at the highest rate
- ESC-derived pups, apart from S/L, develop tumor-like structures later on
- Chemical-based media suppress Hox family genes and imprinted genes

Authors

Chenglei Tian, Jing Wang, Xiaoying Ye, ..., Jichang Wang, Guoping Fan, Lin Liu

Correspondence

wangjch53@mail.sysu.edu.cn (J.W.), guopingfan@gmail.com (G.F.), liulin@nankai.edu.cn (L.L.)

In brief

Tian et al. found that culture conditions affect ESC pluripotency and long-term differentiation potential. Conventional serum/Lif ESC cultures produce more healthy pups than do chemical-based ESC cultures, and current chemical-based media prompt the development of atypical teratomas later on. Chemical-based media suppress Hox family and imprinted genes.

Tian et al., 2023, Cell Reports *42*, 112645
June 27, 2023
https://doi.org/10.1016/j.celrep.2023.112645

CellPress

Cell Reports

CellPress
OPEN ACCESS

Article

Culture conditions of mouse ESCs impact the tumor appearance *in vivo*

Chenglei Tian,[1,2,7,8] Jing Wang,[3,8] Xiaoying Ye,[1,2,8] Jiyu Chen,[1,2,8] Rongyan Zheng,[4,8] Hanwen Yu,[4] Jie Li,[1,2] Guoxing Yin,[1,2] Linlin Liu,[1,2] Nannan Zhao,[2] Guofeng Feng,[1,2] Zhengmao Zhu,[1,2] Jichang Wang,[4,*] Guoping Fan,[3,6,*] and Lin Liu[1,2,5,9,*]

[1]State Key Laboratory of Medicinal Chemical Biology, Nankai University, Tianjin 300071, China
[2]Frontiers Science Center for Cell Responses, College of Life Sciences, Nankai University, Tianjin 300071, China
[3]Department of Human Genetics and Broad Stem Cell Research Center, David Geffen School of Medicine, University of California Los Angeles, Los Angeles, CA 90095, USA
[4]Key Laboratory for Stem Cells and Tissue Engineering, Zhongshan School of Medicine, Sun Yat-sen University, Guangzhou 510080, China
[5]Institute of Translational Medicine, Tianjin Union Medical Center, Nankai University, Tianjin 300071, China
[6]Shanghai Institute for Advanced Immunochemical Studies, ShanghaiTech University, Shanghai 201210, China
[7]Present address: Institute of Translational Stem Cell Research, Helmholtz Diabetes Center, Helmholtz Zentrum München, Ingolstädter Landstraβe 1, 85764 Oberschleiβheim, Germany
[8]These authors contributed equally
[9]Lead contact
*Correspondence: wangjch53@mail.sysu.edu.cn (J.W.), guopingfan@gmail.com (G.F.), liulin@nankai.edu.cn (L.L.)
https://doi.org/10.1016/j.celrep.2023.112645

SUMMARY

Various culture conditions by small molecules have been explored to extend pluripotency of stem cells, but their impacts on cell fate *in vivo* remain elusive. We systematically compared the effects of various culture conditions on the pluripotency and cell fate *in vivo* of mouse embryonic stem cells (ESCs) by tetraploid embryo complementation assay. Conventional ESC cultures in serum/LIF-based condition produced complete ESC mice and also the survival to adulthood at the highest rates of all other chemical-based cultures. Moreover, long-term examination of the survived ESC mice demonstrated that conventional ESC cultures did not lead to visible abnormality for up to 1.5–2 years, whereas the prolonged chemical-based cultures developed retroperitoneal atypical teratomas or leiomyomas. The chemical-based cultures exhibited transcriptomes and epigenomes that typically differed from those of conventional ESC cultures. Our results warrant further refinement of culture conditions in promoting the pluripotency and safety of ESCs in future applications.

INTRODUCTION

Mouse embryonic stem cells (mESCs) were originally established by culture in serum/LIF in the presence of feeder cells.[1] Notably, these conventional embryonic stem cell (ESC) cultures exhibit heterogeneous expression of pluripotent genes and sporadically enter a two-cell-like state as shown by expression of Zscan4 for telomere elongation[2] as well as by fluctuation of endogenous retrovirus activity.[3] There has been intensive interest in pursuing extending pluripotency of ESCs or pluripotent stem cells (PSCs) for maximizing their potential clinical therapy in regenerative medicine. During the exploration of simplified cultures without serum and feeders, excitingly, 2i (MEK and Gsk3 inhibitors)/LIF can also maintain pluripotent mESCs and further promote to ground state by inducing relatively homogeneous expression of pluripotent genes.[4] Further refinement of the 2i/LIF medium by replacement of the Mek1/2 inhibitor with an Src inhibitor (a2i/LIF) preserves the epigenetic and genomic integrity as well as the developmental potential of mESCs.[5,6] These mESCs exhibit the potential to develop into three embryonic germ layers. Meanwhile, extending pluripotency by a chemical cocktail enables the developmental potential of both embryonic and extraembryonic lineages.[7] Tetraploid embryo complementation (TEC) for supporting extraembryonic development assay demonstrates that mESCs are able to develop into all cell types in an entire organism as shown by complete ESC mice and has been commonly accepted as the most stringent test of developmental pluripotency of PSCs.[8] All these various ESC cultures can generate complete ESC pups by TEC assay, demonstrating that they are developmentally pluripotent, including conventional ESC cultures in serum/leukemia inhibitory factor (LIF) in the presence of feeders[1,9–11] and also iPSCs,[12,13] chemical-based ESC cultures such as 2i/LIF (LIF+CHIR99021+PD0325901) or a2i/LIF (LIF+CHIR99021+CGP77675),[4–6,11,14] and LCDM (LIF+CHIR99021+Dim+Mih) cultures.[7,15] However, direct comparisons of the effects of various culture conditions on developmental potential and the cell fate *in vivo* of ESCs from the same genetic background in live animal models have not been examined for the longer term.

On the other hand, there have been concerns about the risk of teratoma formation and tumorigenesis in ESC derivatives,[16–20] but effectively testing the concerns requires appropriate models.

While the directed differentiation and cell transplantation and tracing have been informative in assessing the specific cell lineage, fate, and function,[21] ESC mice derived by the TEC method could provide an appropriate model for evaluating the long-term fate and function of ESCs at the whole-organismal levels. Here, we generated complete ESC mice through TEC assays of various ESC cultures, including serum/LIF-based and chemical-based conditions, and examined the health status of the mice for between 1.5 and 2 years.

RESULTS

Derivation and maintenance of mESCs at various culture conditions

We derived ESCs from the same mouse genetic background and maintained the ESC cultures under conventional serum/LIF and feeder conditions (S/L),[1,9,22] 2i or a2i with feeders (2iL or a2iL)[5] or without feeders (2iL-F) for achieving ground state,[4] or LCDM-based condition for extended PSCs (EPSCs)[7] (Figures 1A, S1A, and S1B). The ESC lines #3 and #5 represented two biological repeats of independent experiments. Side-by-side comparisons of molecular markers for conventional mESCs, ground-state ESCs and EPSCs showed that these ESCs highly and ubiquitously expressed pluripotent Oct4 protein, regardless of conventional, 2i, a2i, or LCDM-based cultures by immunofluorescence (Figure 1B). Expression of Nanog varied among various culture conditions. Nanog was homogenously expressed in LCDM and 2i cultures but heterogeneously expressed in conventional ESC and a2i cultures. Interestingly, the cell surface marker SSEA1, typical for naive pluripotency, was expressed at higher levels in ESCs under conventional S/L and LCDM culture conditions, unlike that of 2iL, a2iL, and 2iL-F cultures (Figure 1B).

Efficiency and survival of the ESC mice completely produced by TEC

To assess the developmental potential of pluripotent ESCs, we generated all ESC mice by TEC assay from various ESC cultures at passage 5 or 10. Side-by-side functional comparisons of conventional ESCs, ground-state ESCs, and EPSCs showed that various ESCs by passage 5 (P5) produced all-ESC-derived fertile pups via TEC (Figures 2A and 2B). Conventional ESCs produced full-term ESC pups at an efficiency of 30.0%, significantly higher ($p < 0.05$) than that of 2iL, a2iL, or LCDM cultures on the feeder cells, respectively. Moreover, all ESC pups produced from conventional ESCs survived to adulthood (count at about 1 month old), but about half of the ESC pups from 2iL, a2iL, or LCDM-based cultures failed to survive to adulthood. The survival rate of the mice from those chemical-based cultures also was lower ($p < 0.05$ or 0.01) than that of serum/LIF-based cultures (Figure 2A).

We further compared the efficiency in the production of ESC mice and their survival to the adulthood by various cultures at passage 10. Conventional ESCs at passage 10 produced full-term ESC pups at an efficiency of 12.1%, not different from that of 2iL- or a2iL-based medium, respectively, but higher than ($p < 0.05$ or 0.01) those of 2iL-F and LCDM cultures (Figures 2A and 2B). While the survival rate of ESC mice from a2iL cultures (8.6%) did not differ from that of serum/LIF cultures, no pups survived to adulthood from ESCs of 2iL and LCDM cultures.

The juvenile mice that failed to survive did not exhibit visible abnormality and did not develop any tumors/teratomas by dissection. All ESC pups were validated by microsatellite genotyping, indicating their originality of the ESCs but not of donor mice providing tetraploid embryos (Figure 2C). The ESC mice had germline competence as shown by producing healthy offspring (Figures 2A and 2D). In addition, EPSCs from LCDM cultures can generate all-ESCs mice with germline capacity through single-cell injection by TEC assay (our preliminary data).

Previously, ESCs in C57BL/6J×CBA genetic background at early passages maintained under S/2i/L condition could generate live-born pups. However, the ESC pups failed to survive to adults. Moreover, the ESCs after extended cultures under S/2i/L condition could not give rise to live-born pups.[11] These data are consistent with those of the 2i condition of ESCs in another genetic background reported here (Figure 2A), indicating that prolonged 2i cultures impair healthy development regardless of the serum. ESC mice also could be produced by TEC assay from a2iL cultures for more than 10 passages.[5] Failure in producing all ESC mice from prolonged 2i cultures was attributed to the chromosomal instability resulting from sustained genome-wide hypomethylation.[5] These results implied that prolonged cultures in chemical-based media could impair developmental potential.[5,6] However, the conventional ESCs generate ESC mice by TEC assay at higher efficiency and higher survival rate, compared with those of ESCs maintained in the chemical-based media.

Tumor-like structure formation in ESC mice produced from ESCs maintained in chemical-based cultures

The ESC mice were raised for up to 2 years for further examination of their health. When all ESC mice grew to 1.5–2 years old, surprisingly, all 9 ESC mice produced from ESCs maintained in chemical-based cultures for ground state or extended pluripotent state formed retroperitoneal tumor-like structures (Figures 3A and 3B), whereas all seven ESC mice produced from conventional ESCs cultured in serum/LIF on the presence of feeders did not exhibit any visible abnormality. The diameter of the tumor-like structures was about 0.7–1.5 cm, and the diameter of tumors formed in ESC mice from LCDM cultures appeared to be relatively dark red and larger (Figure 3B). As all the four groups of chemical-based media produced similar tumor-like structures and shared CHIR99021 to activate Wnt signaling, we combined these groups for comparison of tumor-like formation with that of serum/LIF-based media. By statistics analysis using Fisher's exact test, the frequency of tumor-like structures formed from chemical-based cultures differed significantly ($p < 0.0001$) from that of conventional ESC cultures (Figure 3C).

To discern the nature of tumor-like structures developed in the ESC mice from ground-state ESCs or EPSCs, we performed H&E staining of the sections and compared them with the teratomas formed at approximately 1 month by standard teratoma assay for the differentiation capacity following subcutaneous injection of ESCs into immunodeficient mice. Standard teratoma

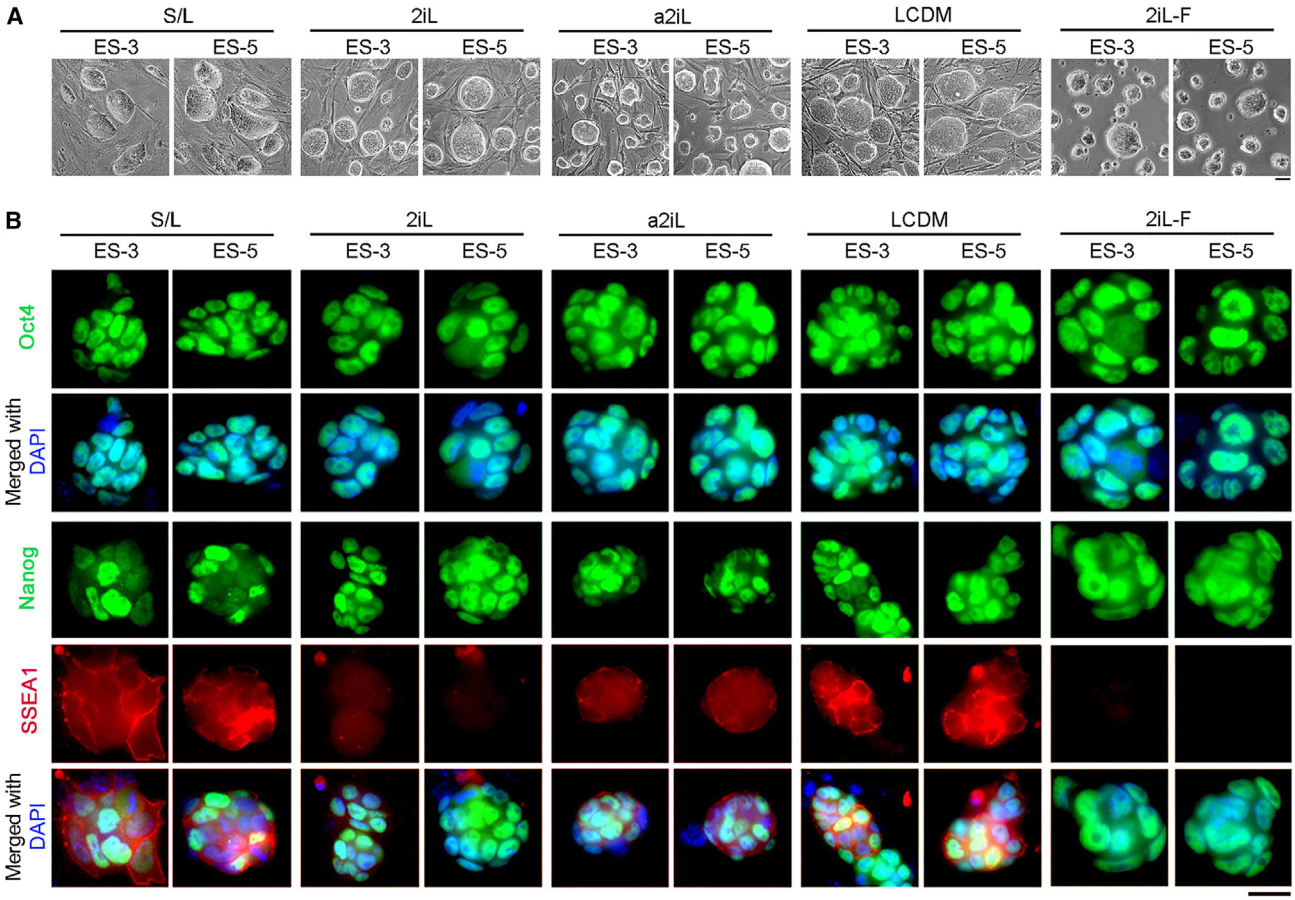

Figure 1. Comparison of various ESC cultures

(A) Representative morphology of mESCs maintained at various pluripotent states by cultures in various conditions at passage 10 (P10) under bright-field with phase-contrast optics. #3 and #5 represent two biological repeats of ESC lines derived from different ESC clones. Scale bar, 100 μm.

(B) Immunofluorescence microscopy of pluripotent markers, Oct4, Nanog, and SSEA1, showing the expression pattern in ESCs at P10 under various culture conditions. Scale bar, 20 μm. See also Figure S1.

formation contained three embryonic germ layers in the sections (Figure S2A), which are typically marked by βIII-tubulin for neuronal ectoderm, alpha-smooth-muscle actin (αSMA) for mesoderm, and α-fetoprotein (AFP) for endoderm (Figure S2B). Nevertheless, tumor-like structures or teratomas that developed in the ESC mice did not exhibit obvious neuronal ectoderm by lack of βIII-tubulin immunofluorescence, nor endoderm differentiation by AFP staining, except for the LCDM tumor (Figure S2B). One of prominent structures in the tumor-like structures of the ESC mice manifested robust αSMA staining, indicative of myocytes, vascular smooth-muscle cells, or myofibroblasts around the inside of the tumor-like structures from 2iL or a2iL ESCs or mixed in the tumor of LCDM ESC-derived mice, quite similar to the mesoderm lineage in the standard teratomas (Figures 3D, 3E, S2, and S3). Furthermore, we characterized the tumor-like structures using additional markers glial fibrillary acidic protein (GFAP) for detecting astrocytes and glial cells,[23] and P63 for epidermal development of ectoderm.[24] The standard teratomas were stained by typical GFAP filament structures and nuclear or cytoplasmic P63, and the tumor-like structures from ESC mice did not have GFAP filaments but expressed nuclear or cytoplasmic P63 (Figure S4).

Collectively, these data show that extending pluripotency by prolonged cultures in chemical-based media not only compromises the full-term developmental potential of ESCs and survival of the pups but also can lead to formation of atypical teratomas or leiomyomas in the derived ESC mice that contain mesoderm, epidermal ectoderm, and occasionally endoderm.

Distinct transcriptome profile of various ESC cultures

To understand the molecular basis for the differences in the developmental pluripotency and formation of the atypical teratomas, we performed systematic comparative analysis of various ESC cultures by RNA sequencing (RNA-seq), exome sequencing, assay for transposase-accessible chromatin with sequencing (ATAC-seq), and telomere measurement. The genome-wide gene expression profile could distinguish the five different ESC cultures (Figure 4A). Expression levels of pluripotency genes varied among the five culture conditions (Figure 4B). *Oct4* and *Dppa4* mRNA levels did not differ among them. While

A

Passage	Condition	Feeder	No. embryos transferred	Full-term (%)	Adult (%)	Germline competence
P5	S/L	Yes	40	12 (30.0%)	12 (30.0%)	Yes
	2iL	Yes	27	2 (7.4%) *	1 (3.7%) *	Yes
	a2iL	Yes	60	8 (13.3%) *	5 (8.3%) **	Yes
	LCDM	Yes	41	4 (9.76%) *	2 (4.88%) **	Yes
	2iL	No	19	4 (21.1%) ns	2 (10.5%) ns	Yes
P10	S/L	Yes	66	8 (12.1%)	6 (9.1%)	Yes
	2iL	Yes	65	2 (3.2%) ns	0 (0.0%) *	NA
	a2iL	Yes	35	4 (11.4%) ns	3 (8.6%) ns	Yes
	LCDM	Yes	44	0 (0.0%) *	0 (0.0%) *	NA
	2iL	No	59	0 (0.0%) **	0 (0.0%) *	NA

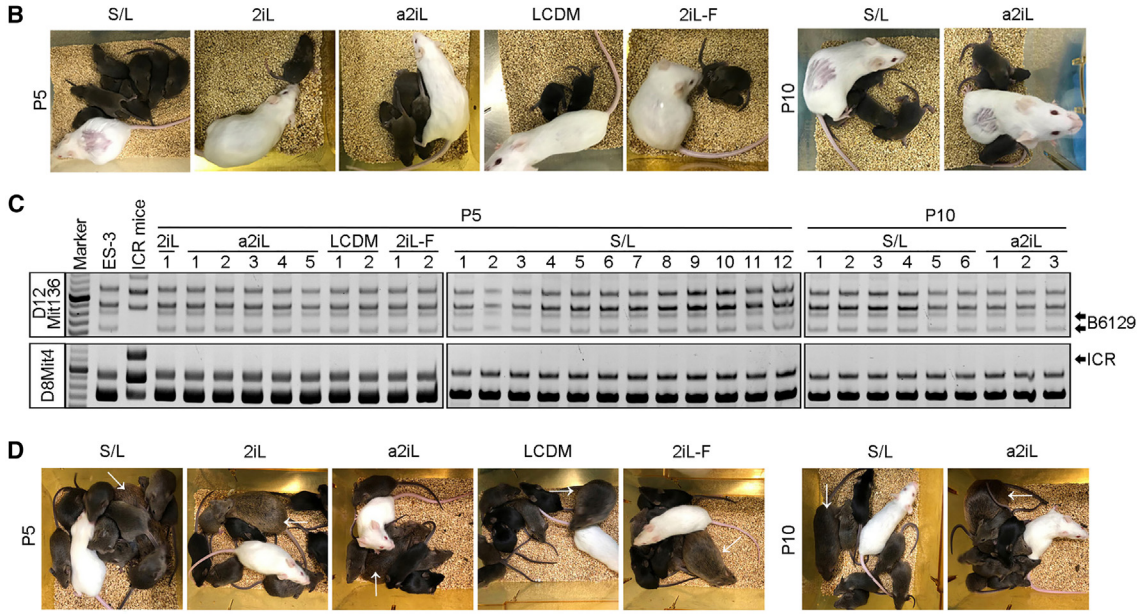

Figure 2. Developmental potential of ESCs by TEC assay

(A) Summary of the ESC mice produced by TEC of various ESC culture conditions at P5 and P10. Ten ESCs were injected into the tetraploid blastocysts made and developed from the fusion of two-cell embryos of albino ICR mice, followed by embryo transfer. MEFs served as feeder cells. Statistics by chi-squared test or Fisher's exact test to examine the differences in the live efficiency at full term or the survival to the adulthood from chemical-based cultures, compared with S/L-based cultures. *$p < 0.05$; *$p < 0.01$; ns, not significant. Details are provided in Table S1.

(B) ESC pups created by TEC exhibit black coat color.

(C) Microsatellite genotyping analysis showing contributions of ESCs, but not ICR TEC embryos, to the produced pups. Upper is D12Mit136 and lower is D8Mit4.

(D) ESC mice generated by TEC assay and the germline competence as shown by offspring (coat color in black) produced from the ESC mice of various ESCs at P5 and P10. ESC mouse (indicated by white arrow) was crossbred with albino mouse. See also Figure S1 and Table S1.

some pluripotent genes (e.g., *Dppa2*, *Lin28a*) were expressed at higher levels, others, such as *Sox2*, *Tbx3*, *Nanog*, *Essrb*, and *Klf5*, expressed at relatively lower levels in S/L ESCs compared with those of chemical-based cultures. Nanog protein was highly expressed in LCDM and 2iL cultures but expressed at relatively lower levels in conventional ESC and a2iL cultures, while Lin28a expression exhibited the opposite pattern (Figure 4C). Like mRNA expression, protein levels of *Dnmt3a/b* appeared to be lower in the 2iL and a2iL cultures compared with conventional serum-based cultures (Figure 4D). Lower *Dnmt3a* protein levels were also found in a2iL and LCDM than in S/L cultures. Consistently, conventional ESC cultures exhibited 5-methylcytosine (5mC) at a higher level than those of chemical-based cultures, despite relatively stable lower 5-hydroxymethylcytosine (5hmC) levels in all cultures (Figure 4E), further verifying the global hypomethylation in the 2i-based cultures.[5,6]

By Kyoto Encyclopedia of Genes and Genomes (KEGG) enrichment analysis of differentially expressed genes (DEGs), several essential signaling pathways differed between S/L and chemical-based ESCs (Figure 4F). The actin cytoskeleton regulation and p53 signaling pathways were notably downregulated in ESCs maintained in chemical-based media, unlike the serum-based ESC cultures (Figure 4G). Proteome analysis also revealed that proteins of integrin and focal adhesion and

A

ESC mice	Cell passage	Age (M)	Tumor
S/L-1	P5	24	0
S/L-2		24	0
S/L-3		24	0
S/L-4		24	0
2iL		19	1
a2iL-1		23	2
a2iL-2		23	1
a2iL-3		23	1
LCDM-1		22	1
LCDM-2		22	1
2iL-F-1		19	1
S/L-1	P10	18	0
S/L-2		18	0
S/L-3		18	0
a2iL		19	1

B

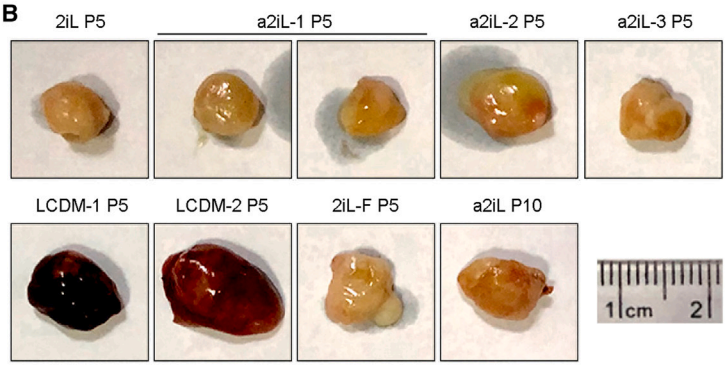

C

Data analysis	Chemicals-based medium	S/L-based medium	Total	Fisher's exact test
Health	0	7	7	P value
Tumor-like	9	0	9	<0.0001
Total	9	7	16	

D

E

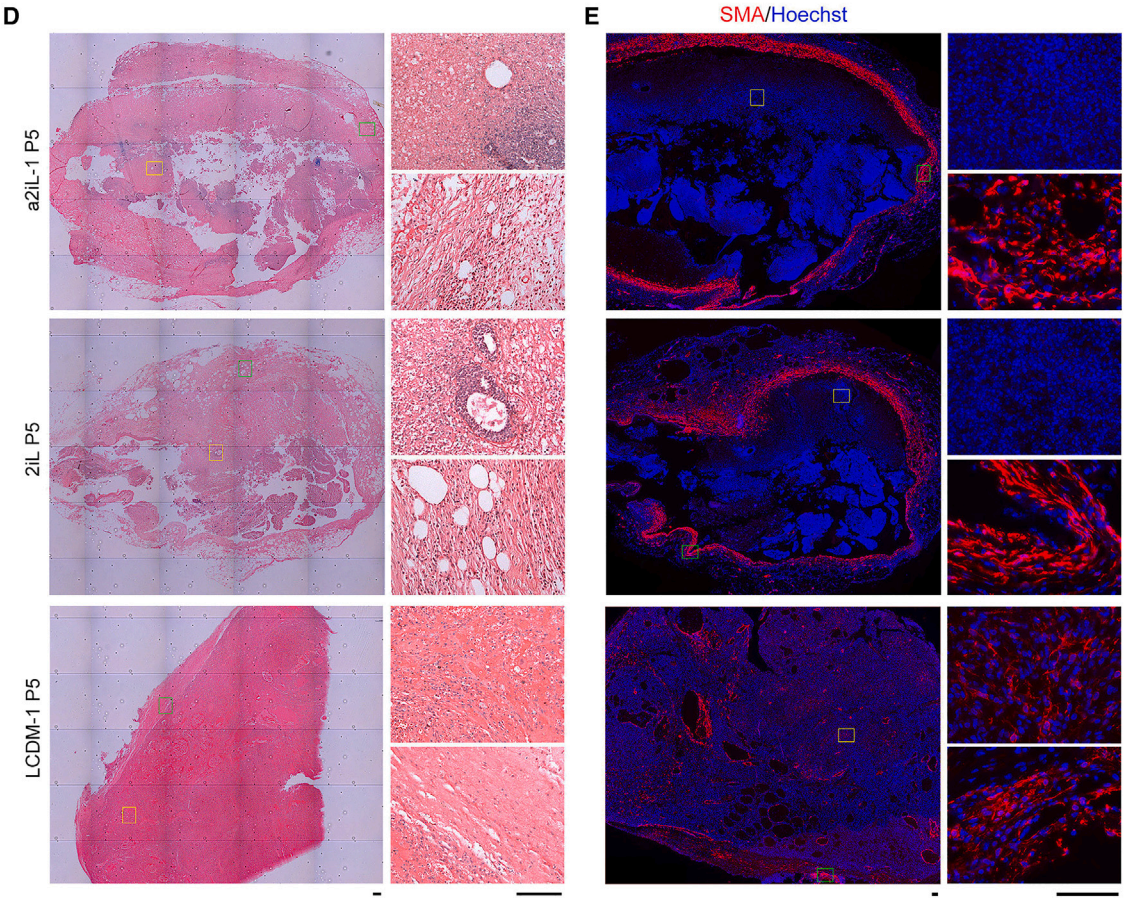

Figure 3. Tumors/teratomas developed in ESC mice produced from chemical-based ESC cultures

(A) While all 9 ESC mice produced from 2iL, a2iL, or LCDM cultures developed tumors, none of the 7 ESC mice produced from conventional ESCs cultured in serum/LIF with feeder (S/L) showed tumors by the age of 18–24 months.

(B) Morphology of tumors collected from intraperitoneal wall of ESC mice produced from ESCs maintained by various chemical inhibitors. Scale bar, 1 cm.

(C) Statistics by Fisher's exact test to examine the differences in the tumor-like formation between S/L-based and chemical-based cultures. ****$p < 0.0001$. Given that all the 4 chemical-based cultures produced similar tumor-like structures and contained CHIR99021 to activate Wnt signaling, these cultures were combined for comparison of tumor-like formation with that of serum/LIF-based media.

(legend continued on next page)

signaling proteins involved in the actin cytoskeleton regulation are enriched in S/L ESCs.[25] In response to the genotoxic stresses, a primary role of p53 in PSCs is to induce the differentiation of PSCs and inhibit pluripotency; the roles of p53 in cellular metabolism might also contribute to genomic stability of PSCs by limiting oxidative stress.[26]

On the other hand, pathways involved in metabolism, such as the tricarboxylic acid (TCA) cycle, pentose phosphate pathway (PPP), glycolysis, and biosynthesis of amino acids, were upregulated in the chemical-based ESC cultures (Figures 4G and S5C). GSK3 inhibition by CHIR99021 promotes mitochondrial respiration in human ESCs.[27] To validate the effect of chemicals on ESCs at the protein expression level, we conducted a proteome analysis using published data from a previous study.[25] A high degree of agreement in the fold changes in gene expression was found between transcriptome (RNA-seq) and proteome analyses (Figure S5A). Specifically, when comparing the chemical-based ESCs (2iL) with S/L ESCs, 76.1% of the downregulated genes and 76.7% of the upregulated genes showed consistent expression changes at both the RNA and protein levels (Figure S5B). The observed discrepancies in gene expression changes likely suggest the presence of post-transcriptional regulation mechanisms. Moreover, the proteome analysis confirmed the downregulation of the actin cytoskeleton pathway and the upregulation of metabolic pathways in the chemical-based ESCs (2iL) (Figure S5C). In support, the 2i condition elevates mammalian target of rapamycin (mTOR), mitochondrial protein components, and metabolism.[28]

Also, *Hox* family genes, particularly Hoxa/b genes, were generally expressed at higher levels in S/L ESCs relative to the ground state or extended ESCs maintained by chemicals (Figure 5A). *Hox* genes are major regulators of animal development and drive stem cell differentiation.[29,30] BMP4-Smad signaling pathway is involved in *Hox* genes expression.[29] Interestingly, BMP4 signaling, important for suppression of ESC differentiation,[31] is highly activated in ESCs cultured in serum/LIF media in the presence of feeder cells.[11] We speculate that relatively active *Hox* genes in S/L cultures may prime ESCs to differentiate efficiently. Additionally, both maternally (e.g., *Cdkn1c*, *Grb10*, *Meg3*) and paternally imprinted genes (*Snurf/Snrpn*, *Mest*, *Peg10*) generally were expressed at lower levels in chemical-based cultures than in serum/LIF cultures (Figure 5B).

Moreover, the DNA recombination pathway was notably upregulated in S/L-based cultures, compared with other cultures, and 2iL without feeders showed the lowest DNA recombination (Figure 5C). Coincidently, S/L ESCs expressed two-cell genes at higher levels than did chemically maintained ESCs (Figure 5C). Immunofluorescence of Zscan4, a representative two-cell gene, revealed expression of Zscan4 protein in approximately 1%–2% of ESC cultures in S/L, 2iL, and LCDM but not in a2iL and 2iL-F cultures (Figure 5D). While two-cell genes were suppressed in 2iL-F, they were sporadically expressed in conventional ESC cultures where Zscan4 was highly upregulated. This result confirmed that feeder cells improved expression of two-cell genes, as previously shown.[11]

Zscan4 elongates telomeres by facilitating telomere recombination.[2] We assessed telomere function in these various ESC lines. Telomerase activity did not differ among various ESC cultures (Figures S6A and S6B). However, telomeres were longer in S/L and LCDM cultures than in 2iL, 2iL-F, and a2iL cultures by passage 10, based on the qPCR method (Figure S6C). Telomere Q-FISH validated longer telomeres in conventional ESC cultures, 2iL on the feeders and EPSCs, compared with those of 2iL-F or a2iL cultures (Figure S6D). Moreover, telomere loss or fragile telomeres and chromosomal fusion were observed in 2iL and a2iL cultures (Figure S6E). Telomere elongation was associated with elevated telomere recombination by telomere chromosome orientation-fluorescence *in situ* hybridization (CO-FISH) assay (Figures S6F and S6G). Together, S/L or LCDM ESC cultures can well maintain telomere functions.

Chromatin accessibility of various ESC cultures

ATAC-seq was performed to further understand the molecular mechanism underlying the distinct transcriptome of various ESC cultures. Thousands of regions were identified with differential chromatin accessibility in the chemical-based cultures compared with S/L conventional cultures, and increased chromatin accessibility regions were significantly enriched in the "enhancer" loci (Figure 5E). Compared with the chromatin accessibility state of the S/L cultures, 2,092 enhancers were identified to be hyperactive in at least one chemical-based medium. Genes closest to these hyper-enhancers were functionally enriched in stem cell proliferation, suggesting that the chemical-based ESC cultures effectively remodel the chromatin structure and accessibility in pluripotency state. Enhancers are frequently bound by transcription factors, and proper activation is essential for regulating pluripotency and self-renewal in ESCs.[32,33] However, the chemical-based cultures decreased chromatin accessibility of *Hox* family genes to various degrees (Figures 5F and 5G), in correspondence with downregulation in the majority of the *Hox* genes (Figure 5A). Moreover, the majority of dysregulated imprinted genes in all chemical-based ESC cultures were downregulated (Figure 5B), accompanied by reduced chromatin accessibility (Figures 5F and 5G).

Hence, prolonged cultures in chemical-based media dramatically remodel chromatin accessibility and thus change the transcriptome, further promoting expression of pluripotent genes but notably suppressing *Hox* family genes as well as imprinted genes, in contrast to conventional ESC cultures. Both a2iL and 2iL-F seem to minimally express two-cell genes and particularly

(D) Representative sections reconstituted from individual images by H&E staining of the tumors developed in mice produced from various ESCs by TEC. Three representative tumors are shown. The other 5 tumors are provided in Figure S4. Scale bar, 100 μm. The whole tumor images (left) were taken by the laser microdissection system LMD6000 and merged automatically.

(E) Immunofluorescence of αSMA in the section of the tumors from ESC mice. Blue, nuclei stained by Hoechst 33342. About 11–21 images depending on the size of the tumors were taken with 5× lens by Zeiss imager Z2 and stitched into a complete picture using Photoshop software. The picture on the upper right is the area at high magnification delineated by a yellow frame in the image at low magnification on the left. The picture at the bottom right is the area at high magnification delineated by a green frame. Scale bar, 50 μm. See also Figures S2–S4.

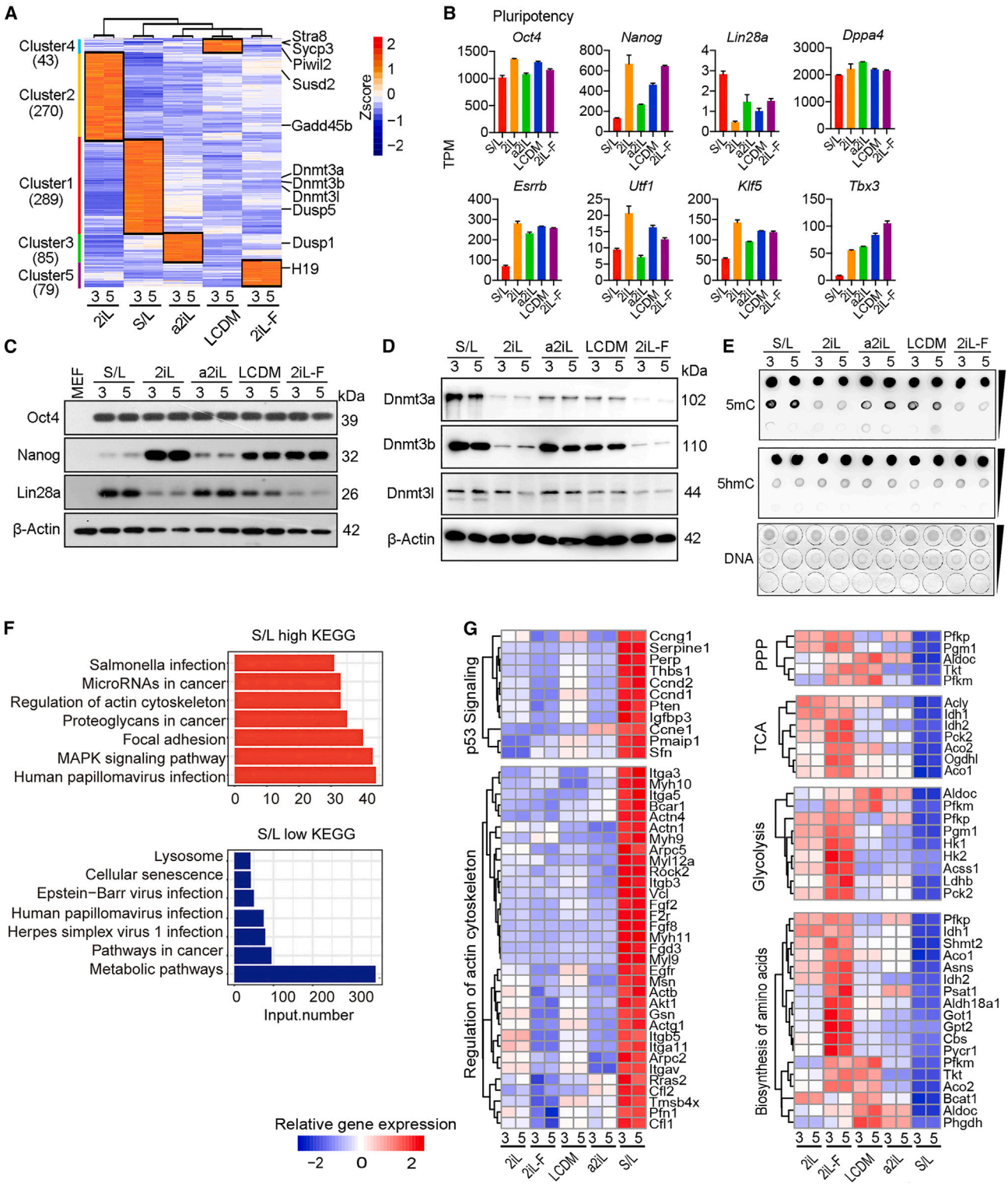

Figure 4. Distinct transcriptome by RNA-seq of ESCs under various culture conditions

(A) Heatmap illustrating clusters of representative genes expressed at a higher level in various ESC cultures at P10.

(B) Expression levels by RNA-seq of key pluripotency-related genes in various ESC cultures at P10.

(C) Protein levels of typical pluripotent markers, Oct4, Nanog, and Lin28a in ESCs maintained at various conditions by western blotting; β-actin served as loading control.

(legend continued on next page)

Zscan4 (Figures 5C and 5D). However, compared with a2iL, 2iL-F may cause abnormal embryonic development due to the combination of decreased two-cell-stage genes, telomere shortening, as well as abnormal epigenetic changes including methylation (Figures 4D, 4E, and 5E–5G).

Whole-exome sequencing of the ESC cultures and teratomas

To test whether the genomic instability is also potentially implicated in the reduced pluripotency by TEC and the increased teratoma formation from chemical-based cultures, we performed whole-exome sequencing of the ESCs maintained at various conditions as well as of the corresponding teratomas. The teratomas in the mice generated from ESCs under chemical-based cultures did not show many differences in the number of copy number variations (CNVs), single-nucleotide variants (SNVs) in coding sequence (CDS), and indels in CDS (Figures 6A and 6B). Teratomas from LCDM ESCs at P5 exhibited more CNVs in chromosome 2 and chromosome 16 and 18, and a2iL ESCs at P5 in chromosome 15 (Figure 6B). The number of CNVs, SNVs in CDS, and indels in CDS also did not differ among various ESC cultures (Figure 6C). ESCs under 2iL-F cultures resulted in more genes contained in the CNVs, distinct from the other four culture conditions. ESCs under 2iL-F cultures exhibited more CNVs in chromosome 8 (Figure 6D). The number of SNVs in CDS of ESCs was generally lower than that of the teratomas (Figure 6C vs. 6D). CNVs located in the genome of ESCs differed from those of the teratomas (Figures 6B and 6D).

To further examine whether the mutations and CNVs were shared between the ESCs and teratomas, we compared the genomic sequencing data of the chemical-based ESC cultures using the conventional S/L ESC cultures as the same reference control, given that the conventional ESC cultures produced ESC mice that had no visible abnormalities. Based on the analysis methods described previously,[34,35] very few mutations were shared between the teratomas and their progenitor ESCs, and the proportion of mutations in the same ESCs and teratomas was quite low when either conventional ESCs from two independent repeats #3 or #5 served as reference control (Figure 6E). Among them, mutations of *Nlrp1b*, *Mid1*, and *Arpp21*, etc. were more frequently observed in ESCs and/or teratomas. *NLRP1* is an essential mediator of the host immune response through modulating interleukin (IL)-1β and IL-18 levels in the colon.[36] *ARPP21*, as an RNA-binding protein, encoded by the host gene of miR-128-2, antagonized miR-128 activity by competing with it to bind to the 3′ untranslated region (UTR) of Ppp1cc to maintain the balance of the differentiation state of myoblasts.[37] CNVs appeared to differ between the ESCs and teratomas, and the teratoma generally had more chromosomal deletions than did ESCs and the trend remained the same for the conventional ESCs serving as reference control in two repeated experiments (Figure 6F). Together, the exome sequencing reveals only subtle differences in the CNVs, SNVs, and mutations among the various ESC cultures. These data suggest that the genomic mutations may not significantly contribute, if at all, to the variations in the pluripotency of ESC cultures and the teratoma development in the ESC mice.

Methylome analysis of the teratomas of ESC mice

To investigate the abnormal methylation potentially involved in teratoma formation, we performed reduced representation bisulfite sequencing (RRBS) of the teratomas developed in mice produced from various mESCs by TEC using the abdominal muscle from mice of the same genetic background as controls. Overall, an increase in genomic methylation was found in the teratomas developed in mice produced from various mESCs by TEC compared with that of muscle (Figure 7A). To better define the genomic regions bearing methylation abnormalities in the teratomas, we compared differentially methylated regions (DMRs) between the teratomas and normal muscle. Thousands of DMRs could be identified in each teratoma (Figure 7B). About 3,387 DMRs were shared among the teratomas of all four culture conditions, reflecting the common epigenetic perturbation in the teratoma formation (Figure 7B).

Genomic imprinting is essential for development but is unstable in PSCs.[38] It was shown that prolonged culture of male ESCs in 2iL causes erosion of genomic imprinting, which impairs developmental potential.[5] We noticed that dozens of imprinted genes exhibited abnormal DNA methylation in the teratoma tissues (Figure 7C). Consistently, the expression of the imprinted genes was dysregulated in the ESCs (Figure 7C), implying the consistent perturbation of genomic imprinting in the chemical-based ESCs and the corresponding teratomas. By comparing the imprinting status of each condition, we attempted to find the common abnormal genomic imprinting shared by all teratomas. We identified 23 imprinted genes that exhibited abnormal DNA methylation and all of them were hypermethylated (Figure 7D). For instance, the promoter and gene body of maternally imprinted gene *Cdkn1c* had higher methylation levels in the teratomas than in the muscle, while the increased methylation levels occurred only in the gene body of *Grb10* in tumors (Figure 7E). The gene bodies of two key paternally imprinted genes (*Snurf* and *Snrpn*) showed increased methylation levels in the teratomas compared with those of the muscle (Figure 7E).

Cells expressing Oct4 found in the teratomas of ESC mice

Additionally, we tested the possibility of retaining pluripotent cells implicated in the teratoma development.[39] A select set of core transcription factors in combination governs and thereby defines pluripotency: OCT4 (also known as POU5F1), SOX2, and NANOG.[8,33] To reveal any potential pluripotent cells in the teratomas, we performed immunofluorescence microscopy of

(D) Protein levels of Dnmt3a, Dnmt3b, and Dnmt3l are higher in S/L, a2iL, and LCDM ESCs than in 2iL and 2iL-F ESCs by western blotting.
(E) Relative quantification of 5mC and 5hmC levels of ESC cultures by dot blotting.
(F) The bar plots showing the KEGG enrichment analysis of the upregulated (top) and downregulated genes (bottom) in S/L ESCs compared with chemical-based ESCs.
(G) Heatmap displaying the differently expressed genes involved in selected essential pathways between chemical-based and S/L ESCs. See also Figure S5.

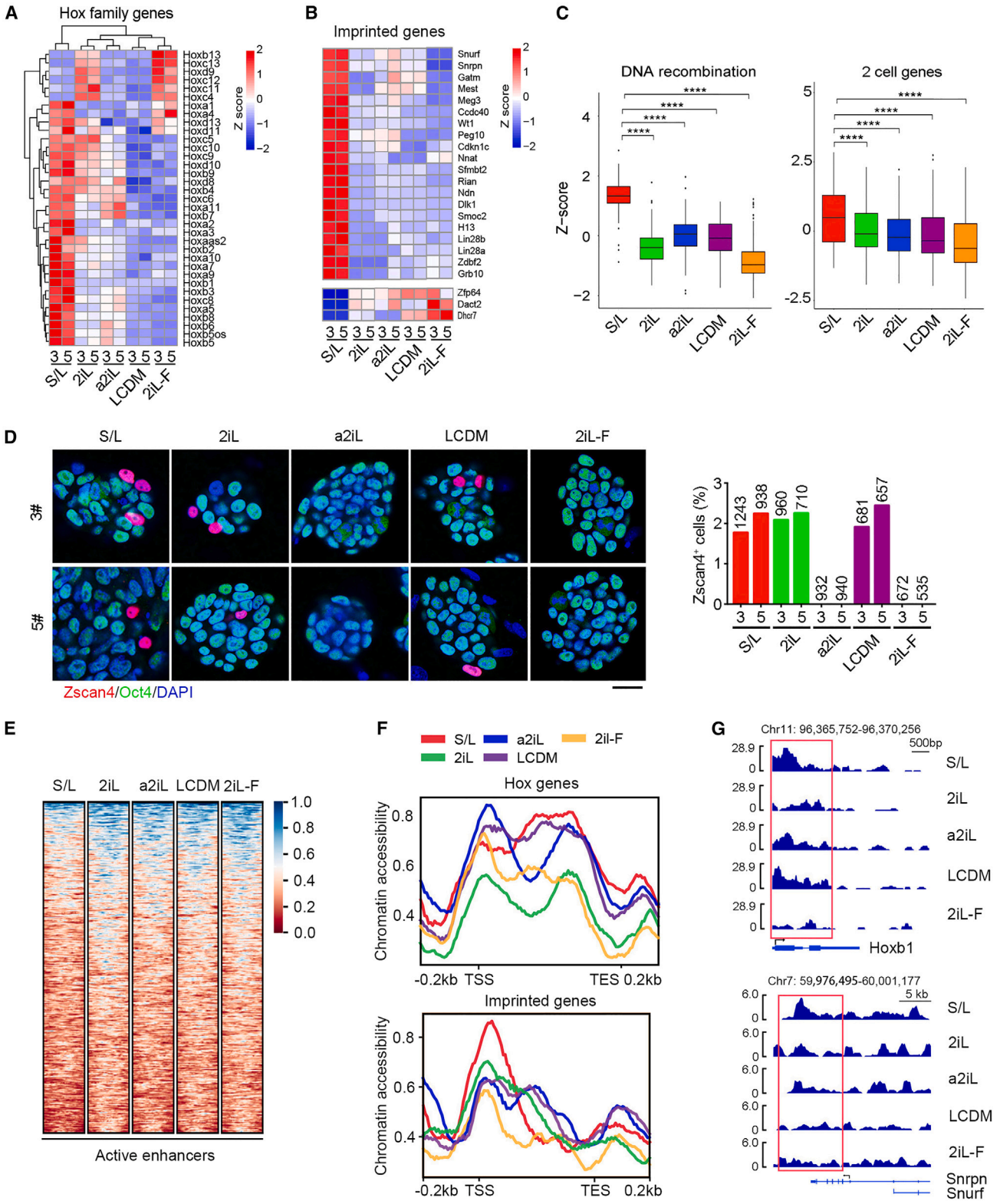

Figure 5. Distinct transcriptome linked to chromatin accessibility of ESCs

(A) Expression profile of *Hox* family genes in various ESC cultures at P10.

(B) Heatmap showing expression of common imprinted-related DEGs identified in all chemical inhibitor-based ESCs compared with the ESCs in S/L condition.

(legend continued on next page)

the key pluripotent marker genes Oct4, Nanog, and Sox2 using ESCs as positive controls. Notably, Oct4 was expressed in the cells, despite few of the teratomas formed in ESC mice (Figure S7). Oct4-positive cells varied among the tumors of different ESCs, and the teratomas developed in mice from a2iL or 2iL-F had more Oct4-positive cells (Figure S7). Sox2 was expressed in the standard teratomas but not in the teratomas of the ESC mice. It remains unclear whether these escaped PSCs could also contribute to the formation of teratomas.

DISCUSSION

Criteria of increasing stringency are proposed to determine the developmental potential of expanded or extended pluripotency.[40] Using TEC assay and by direct comparison, we demonstrate that conventional serum/LIF-based ESC cultures produce all ESC mice with the survival at higher rate than do other chemical-based ESC cultures; meanwhile, these data also support the notion that the ESCs are very effective in differentiation into all cell types in the body as well being very safe. Based on TEC assay, the conventional serum/LIF-based ESC cultures still remain the most pluripotent of stem cells, compared with the "extended" pluripotent state achieved by current chemical-based cultures. Moreover, the conventional ESC cultures can differentiate completely into all cell types in the body without the risk of tumor or teratoma formation. By contrast, prolonged ESC cultures maintained by the current chemicals could lead to atypical teratoma formation. Extending pluripotency by chemical-induced epigenetic remodeling turns out to be more about transcriptional regulation rather than genomic stability. Genomic analysis did not detect obvious differences in CNV, SNP, and indel among these ESC cultures. These data suggest that epigenetic alterations (e.g., DNA hypomethylation) induced by long-term chemical-based culture may link to the reduced development potential and development of atypical teratomas or leiomyomas.

We observed that the teratomas developed in mice produced from ESCs by prolonged chemical-based cultures express Oct4 in few cells. Among the core transcription factors (OCT4, SOX2, NANOG), OCT4 has proven most indispensable and remains the preeminent pluripotency factor.[8] *Oct4* expression is normally confined to pluripotent cells of the developing embryo, including epiblast cells, primordial germ cells, and their *in vitro* counterparts, ESCs and embryonic germ cells, respectively.[41] In addition, *Oct4* is transiently expressed in the developing endoderm[42] and neurectoderm[43] of the embryo, where it may contribute to the specification of cell fate.[44] Downregulation of *Oct4* in ESCs induces trophectoderm differentiation, whereas *Oct4* overexpression induces differentiation into extraembryonic mesoderm and endoderm,[45] demonstrating that Oct4 is a crucial and dose-dependent determinant of pluripotency in embryonic cells.

A mesodermal state is an intermediate state from post-implantation epiblast stem cells advancing to naive pluripotency induction, and Oct4 may precisely regulate this process.[46] Increasing Oct4 also can experimentally induce transdifferentiation of mouse embryonic fibroblasts (MEFs) into cardiac myocytes.[47] Ewing's sarcoma protein can promote Oct4 activity.[48] Additionally, overexpression of *Oct4* shows oncogenic potential in a dose-dependent manner.[44,49] Transduction of OCT4 in normal breast preparations leads to the generation of cell lines possessing tumor-initiating and colonization capabilities.[50] Reactivation of pluripotency-associated genes has been observed in various somatic cancer cells.[51] Intriguingly, Oct4 plays a critical role in balancing the expression of *Hox* family genes.[52] Elevated expression of *Hox* family genes in conventional serum/LIF and feeder cell cultures relative to the chemical-based cultures primes the cells to differentiate, perhaps without retaining undifferentiated cells for potential teratoma formation or tumorigenesis. However, severe suppression of *Hox* family genes in chemical-based cultures may compromise the complete differentiation of a few ESCs, coinciding with the Oct4-expressing cells in the developed teratomas. Oct4-expressing cells may contribute to mesodermal structure formation in the tumors.[46] Extended pluripotency sustained by the small chemicals may compromise complete differentiation of a few perhaps "extremely" pluripotent cells, leading to the existence of pluripotent "escapers" that may also contribute to teratoma formation.

The small chemical compounds that achieve and maintain the ground state or extended pluripotent state induce global hypomethylation and alter chromatin accessibility. The pathways related to cancer and metabolisms are elevated, whereas *Hox* family genes and imprinted genes are preferentially suppressed by the small chemicals. To identify the imprinted genes that are most affected by the culture conditions, we estimated and ranked the p value of all the imprinted genes based on their gene expression (Figure 4B). For top-rank genes, Meg3 suppresses tumor growth and promoter hypermethylation of Meg3 is associated with tumorigenesis.[53–55] Hypermethylation of SNURF/SNRPN is linked to development of teratomas and leiomyoma.[56,57] These imprinted genes are persistently repressed in ESCs and teratoma tissues, suggesting that these aberrant imprinting genes may serve as promising biomarkers for evaluating the atypical teratomas or potential tumorigenicity of the PSCs.

Metabolism plays pivotal roles in cellular physiology, and its interplay with pluripotency has recently attracted broad interest

(C) Expression of DNA recombination and two cell genes in various ESC cultures at P10 shown by boxplot. Data was standardized using *Z* scores of DNA recombination data (GO: 0006310) or two-cell gene lists from 2C::tdTomato$^+$ ESCs (Macfarlan et al.[3]). Kruskal-Wallis was used to compare the differences among the ESC cultures with the R package ggpubr. The lower *Z* score value represents lower gene expression levels. ****$p < 0.0001$.

(D) Immunofluorescence of Zscan4 and Oct4 protein expression in various ESC cultures at P10. Scale bar, 10 μm. Right, proportion (%) of Zscan4-positive cells in an ESC population at P10.

(E) Chromatin accessibility by ATAC-seq at active enhancers of ESC cultures under various conditions.

(F) Average chromatin accessibility at transcription start site across the *Hox* family or imprinted genes of ESC cultures.

(G) Chromatin accessibility on the representative *Hoxb1* gene or *Snrpn/Snurf* differed among various ESC cultures. See also Figure S6.

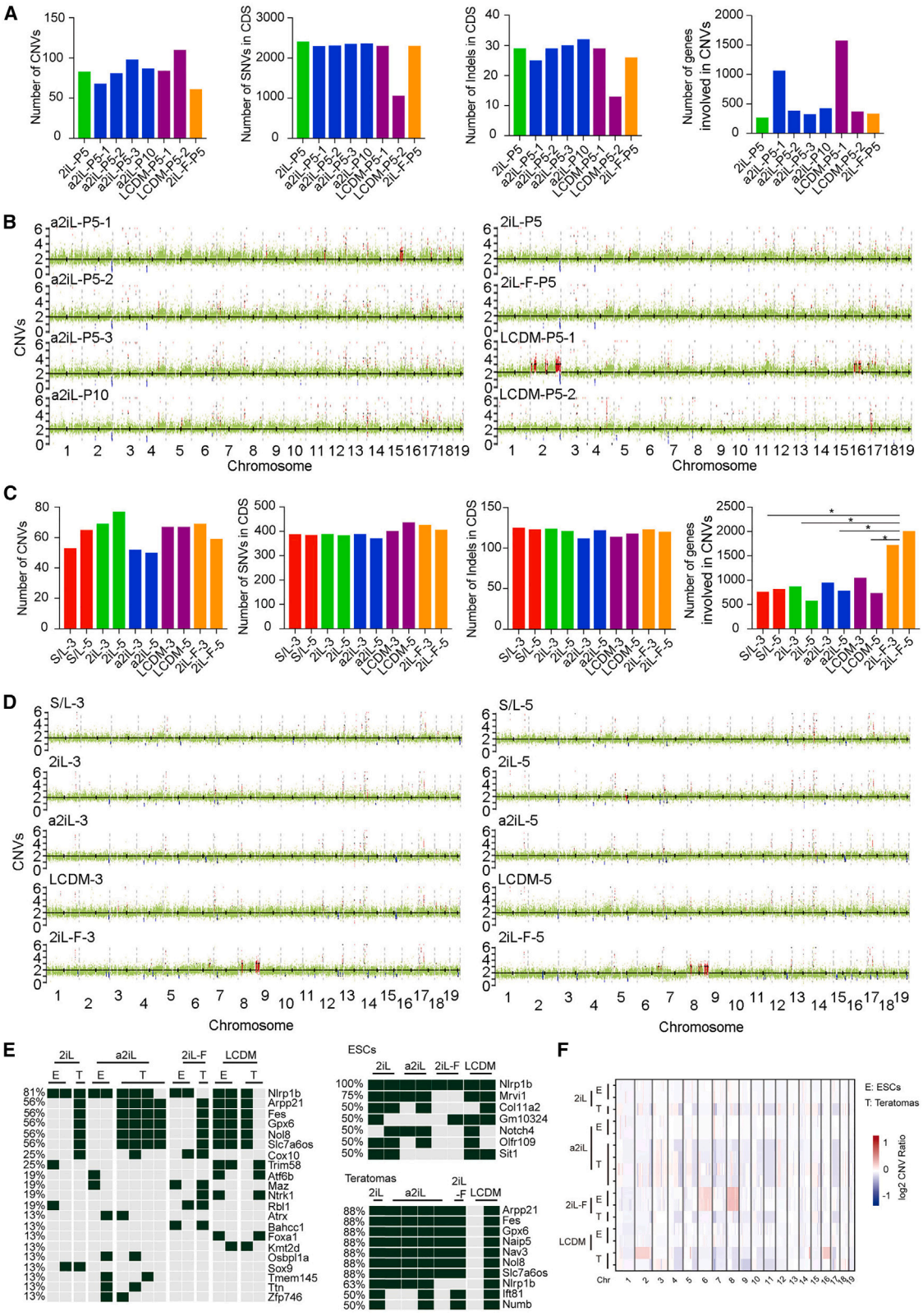

(legend on next page)

in stem cell and cancer biology. The conventional S/L culture condition contains more uncharacterized lipids compared with chemical-based cultures. Lipid lysophosphatidic acid (LPA) is a key modulator that shifts the metabolic landscape without altering pluripotency in human PSCs. LPA may facilitate more closely mimicking physiological conditions during embryogenesis.[58] Pathways related to metabolism are downregulated in S/L ESC cultures, compared with those of chemical-based ESC cultures (Figure 4G). LPA may contribute to the maintenance of the developmental potential of ESCs via regulating cell metabolism under S/L conditions.

Altogether, conventional ESC cultures in serum/LIF-based medium in the presence of feeders, despite their heterogeneous and relatively lower expression of pluripotent genes but elevated expression of *Hox* family genes and imprinted genes for development and differentiation, efficiently generate ESC mice that reproduce and live healthily without tumor formation for up to 2 years, indicating the full developmental potential as well as the safety. Downregulation of metabolic pathways in S/L ESCs may imply their lower energy activity relative to four other ESC cultures maintained by the chemicals. These data from the mouse study could have clinical relevance in regenerative medicine, given that similar chemicals also have been applied to expand the pluripotency of human PSCs/ESCs.

Limitations of the study

Our data suggest that heterogeneous expression of pluripotent genes in serum/LIF-based media does not reduce the pluripotency, with minimal safety issues, unlike what is generally thought. While previous studies showed that reduced MEK inhibition could partially rescue 2i-induced developmental defects of mESCs, our study suggests that chemical-based ESC cultures produce similar tumor-like structures and share CHIR99021 in the media. Thus, it will be interesting to test whether reducing CHIR99021 concentration can rescue the observed defects such as mouse production and tumor formation. In the future, experiments will be needed to identify specific factors, including CHIR99021, and mechanisms that contribute to the declined developmental potential of ESCs and the survival of ESC mice, as well as the atypical teratoma formation from the extended pluripotent ESCs by current chemical approaches. Also, we could not exclude the possibility that the serum itself is the determinant of the quality of the cells.

The mESCs from C57BL/6J×129F1 hybrid strain were used in this study. Earlier experiments also demonstrated that ESCs with another genetic background, C57BL/6J×CBA (carrying Oct4 distal promoter-driven GFP), at early passages maintained in S/2i/L or 2i/L conditions could generate live-born pups, but these ESCs after extended cultures produced pups that failed to survive to adulthood.[11] Future experiments can examine ESCs from more genetic backgrounds to generalize the conclusion and test the transgenerational effects of ESC-culturing conditions. Small chemicals may compromise the complete differentiation of a few perhaps extremely pluripotent cells, such that the pluripotent escapers may contribute to development of the teratoma later on. We obtained and examined the offspring by breeding the ESC mice with ordinary mice. Although we did not see tumors in the offspring at young age (about 1 to 2 months) (Figure 2D), it is unknown whether the mice would develop teratomas if they grew to old age. A continuation of this study to test the hypothesis for future experiments is to analyze the offspring of ESC-derived pups until old age. Additionally, the 2i mice should be bred between them, as the breeding with ordinary mice could dilute the maybe already faint phenotype. The findings reported in this study raise awareness and encouragement for more studies and better *in vivo*-like chemically defined cultures.

Also, it will be worth exploring sex differences in the developmental capacity of ESC mice and their teratoma formation in the future.

STAR★METHODS

Detailed methods are provided in the online version of this paper and include the following:

- KEY RESOURCES TABLE
- RESOURCE AVAILABILITY
  - Lead contact
  - Materials availability
  - Data and code availability
- EXPERIMENTAL MODEL AND STUDY PARTICIPANT DETAILS
  - Mouse ESC
  - Mice
- METHOD DETAILS
  - Tetraploid embryo complementation (TEC) assay
  - Tissue collection and histology
  - Western blot
  - Gene expression analysis by real-time qPCR
  - Dot blot
  - Telomerase activity by TRAP assay
  - Telomerase assay by ELISA

Figure 6. Exome sequencing analysis of ESCs and teratomas

(A) Bar plot showing the number of CNVs, SNVs in CDS, indels in CDS, and genes involved in CNVs in the teratomas developed in ESC mice generated from various ESC cultures.

(B) Distribution of CNVs across the genome in the teratomas. Red color indicates more CNVs.

(C) Bar plot showing the number of CNVs, SNVs in CDS, indels in CDS, and genes involved in CNVs in ESCs under various culture conditions.

(D) Distribution of CNVs across the genome in ESCs under various culture conditions. Red color indicates more CNVs. For genome sequencing analysis of ESC samples, MEFs served as reference control. For genome sequencing analysis of teratoma samples, blood samples from normal mice at the same genetic background served as reference control.

(E) Oncoprint plot shows the same gene mutations in ESCs and teratomas at least in one culture system using S/L ESC-3 as reference control (left). At least 50% of mutations are detected in ESCs and teratomas (right).

(F) Heatmap showing the CNVs in ESCs and teratomas using S/L ESCs-3 as reference control.

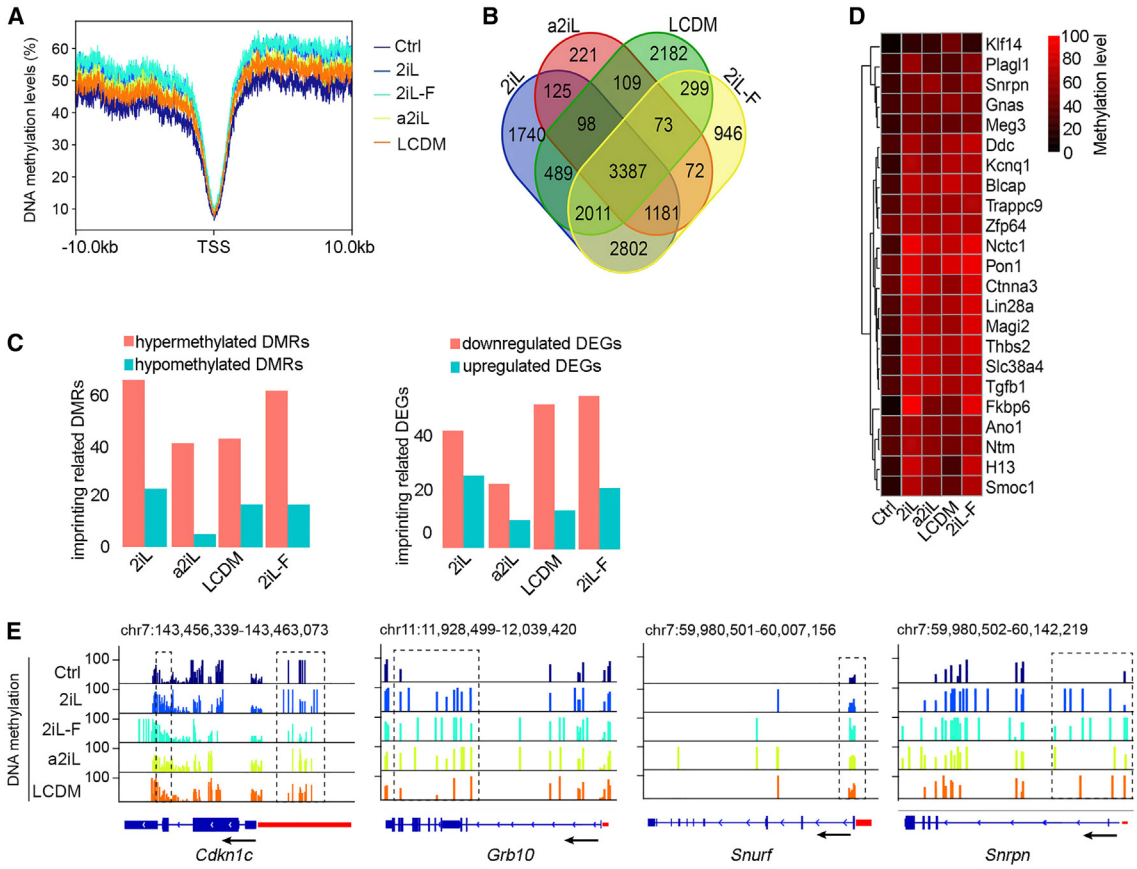

Figure 7. Methylome of the teratomas from ESC mice

(A) Average distribution of CG methylation over RefSeq genes and 10-kb flanking sequences calculated from the RRBS data in abdominal muscle as control (Ctrl) and the teratomas developed in mice produced from various mESCs by TEC. TSS, transcription start site.

(B) Venn plot showing the overlapping genes in the DMRs.

(C) Bar plot showing the imprinting-related DMRs or DEGs identified in tumors derived from various mESCs by TEC.

(D) Heatmap showing methylation of common imprinting-related DMRs identified in various teratoma tissues compared with muscle control.

(E) Methylation pattern of *Cdkn1c*, *Grb10*, and *Snurf/Snrpn* in muscle (Ctrl) and the teratomas developed in mice produced from chemical-based ESC cultures by TEC. RefSeq gene annotations are shown below the tracks; promoter region (red bars, 2 kb upstream from TSS), exons (blue bars), gene direction (black arrow). See also Figures S5 and S7.

- Telomere measurement by real-time qPCR
- Telomere Q-FISH
- Telomere chromosome orientation-fluorescence in situ hybridization (CO-FISH)
- RNA-sequencing and analysis
- ATAC-sequencing and analysis
- Whole-exome sequencing and analysis
- Genome-wide DNA methylation analysis by RRBS

- QUANTIFICATION AND STATISTICAL ANALYSIS

SUPPLEMENTAL INFORMATION

Supplemental information can be found online at https://doi.org/10.1016/j.celrep.2023.112645.

ACKNOWLEDGMENTS

We thank Huasong Wang, Yuan Tian, Kairang Jin, Panpan Shi, Dai Heng, Jiao Yang, and Haifeng Fu for assistance during the experiments; He Ren and Qiang Zhao for advising teratoma analysis; and Haoze Vincent Yu for providing Tn5 enzyme and assisting ATAC-seq sample preparation. This research was supported in part by the National Key R&D Program of China (2018YFA0107000 to L.L. and J.W.), the National Natural Science Foundation of China (82230052 and 32030033 to L.L.), Tianjin Science and Technology Plan Key Project (20JCZDJC00550 to L.L.), and Guangdong Natural Science Foundation (2021A1515010537 to J.W.).

AUTHOR CONTRIBUTIONS

C.T. performed major experiments and data analysis and wrote the manuscript. J.W., G.Y., L.L., J.L., H.Y., and N.Z. carried out bioinformatics analysis. X.Y. performed TEC experiments and germline assays. J.C. performed histology, tissue sectioning, H&E staining, and immunofluorescence microscopy of the sections. G. Feng assisted with western blot and immunofluorescence microscopy of ESCs. R.Z. and H.Y. performed methylome of the teratoma. Z.Z. performed part of the statistical analysis. J.W. and G. Fan discussed the project, supervised the data analysis, and revised the manuscript. L.L. designed the project, supervised the data analysis, and wrote and revised the manuscript.

DECLARATION OF INTERESTS

The authors declare no competing interests.

Received: February 10, 2023
Revised: May 22, 2023
Accepted: May 27, 2023
Published: June 13, 2023

REFERENCES

1. Evans, M.J., and Kaufman, M.H. (1981). Establishment in culture of pluripotential cells from mouse embryos. Nature *292*, 154–156.
2. Zalzman, M., Falco, G., Sharova, L.V., Nishiyama, A., Thomas, M., Lee, S.L., Stagg, C.A., Hoang, H.G., Yang, H.T., Indig, F.E., et al. (2010). Zscan4 regulates telomere elongation and genomic stability in ES cells. Nature *464*, 858–863.
3. Macfarlan, T.S., Gifford, W.D., Driscoll, S., Lettieri, K., Rowe, H.M., Bonanomi, D., Firth, A., Singer, O., Trono, D., and Pfaff, S.L. (2012). Embryonic stem cell potency fluctuates with endogenous retrovirus activity. Nature *487*, 57–63.
4. Ying, Q.L., Wray, J., Nichols, J., Batlle-Morera, L., Doble, B., Woodgett, J., Cohen, P., and Smith, A. (2008). The ground state of embryonic stem cell self-renewal. Nature *453*, 519–523.
5. Choi, J., Huebner, A.J., Clement, K., Walsh, R.M., Savol, A., Lin, K., Gu, H., Di Stefano, B., Brumbaugh, J., Kim, S.Y., et al. (2017). Prolonged Mek1/2 suppression impairs the developmental potential of embryonic stem cells. Nature *548*, 219–223.
6. Yagi, M., Kishigami, S., Tanaka, A., Semi, K., Mizutani, E., Wakayama, S., Wakayama, T., Yamamoto, T., and Yamada, Y. (2017). Derivation of ground-state female ES cells maintaining gamete-derived DNA methylation. Nature *548*, 224–227.
7. Yang, Y., Liu, B., Xu, J., Wang, J., Wu, J., Shi, C., Xu, Y., Dong, J., Wang, C., Lai, W., et al. (2017). Derivation of pluripotent stem cells with in vivo embryonic and extraembryonic potency. Cell *169*, 243–257.e25.
8. De Los Angeles, A., Ferrari, F., Xi, R., Fujiwara, Y., Benvenisty, N., Deng, H., Hochedlinger, K., Jaenisch, R., Lee, S., Leitch, H.G., et al. (2015). Hallmarks of pluripotency. Nature *525*, 469–478.
9. Nagy, A., Rossant, J., Nagy, R., Abramow-Newerly, W., and Roder, J.C. (1993). Derivation of completely cell culture-derived mice from early-passage embryonic stem cells. Proc. Natl. Acad. Sci. USA *90*, 8424–8428.
10. Eggan, K., Akutsu, H., Loring, J., Jackson-Grusby, L., Klemm, M., Rideout, W.M., 3rd, Yanagimachi, R., and Jaenisch, R. (2001). Hybrid vigor, fetal overgrowth, and viability of mice derived by nuclear cloning and tetraploid embryo complementation. Proc. Natl. Acad. Sci. USA *98*, 6209–6214.
11. Guo, R., Ye, X., Yang, J., Zhou, Z., Tian, C., Wang, H., Wang, H., Fu, H., Liu, C., Zeng, M., et al. (2018). Feeders facilitate telomere maintenance and chromosomal stability of embryonic stem cells. Nat. Commun. *9*, 2620.
12. Zhao, X.Y., Li, W., Lv, Z., Liu, L., Tong, M., Hai, T., Hao, J., Guo, C.L., Ma, Q.W., Wang, L., et al. (2009). iPS cells produce viable mice through tetraploid complementation. Nature *461*, 86–90.
13. Kang, L., Wang, J., Zhang, Y., Kou, Z., and Gao, S. (2009). iPS cells can support full-term development of tetraploid blastocyst-complemented embryos. Cell Stem Cell *5*, 135–138.
14. Leitch, H.G., McEwen, K.R., Turp, A., Encheva, V., Carroll, T., Grabole, N., Mansfield, W., Nashun, B., Knezovich, J.G., Smith, A., et al. (2013). Naive pluripotency is associated with global DNA hypomethylation. Nat. Struct. Mol. Biol. *20*, 311–316.
15. Li, R., Zhong, C., Yu, Y., Liu, H., Sakurai, M., Yu, L., Min, Z., Shi, L., Wei, Y., Takahashi, Y., et al. (2019). Generation of blastocyst-like structures from mouse embryonic and adult cell cultures. Cell *179*, 687–702.e18.
16. Ben-David, U., and Benvenisty, N. (2011). The tumorigenicity of human embryonic and induced pluripotent stem cells. Nat. Rev. Cancer *11*, 268–277.
17. Tapia, N., and Schöler, H.R. (2016). Molecular obstacles to clinical translation of iPSCs. Cell Stem Cell *19*, 298–309.
18. Garber, K. (2015). RIKEN suspends first clinical trial involving induced pluripotent stem cells. Nat. Biotechnol. *33*, 890–891.
19. Suman, S., Domingues, A., Ratajczak, J., and Ratajczak, M.Z. (2019). Potential clinical applications of stem cells in regenerative medicine. Adv. Exp. Med. Biol. *1201*, 1–22.
20. Yang, X., Wang, R., Wang, X., Cai, G., Qian, Y., Feng, S., Tan, F., Chen, K., Tang, K., Huang, X., et al. (2018). TGFbeta signaling hyperactivation-induced tumorigenicity during the derivation of neural progenitors from mouse ESCs. J. Mol. Cell Biol. *10*, 216–228.
21. Tabar, V., and Studer, L. (2014). Pluripotent stem cells in regenerative medicine: challenges and recent progress. Nat. Rev. Genet. *15*, 82–92.
22. Williams, R.L., Hilton, D.J., Pease, S., Willson, T.A., Stewart, C.L., Gearing, D.P., Wagner, E.F., Metcalf, D., Nicola, N.A., and Gough, N.M. (1988). Myeloid leukaemia inhibitory factor maintains the developmental potential of embryonic stem cells. Nature *336*, 684–687.
23. Yang, Z., and Wang, K.K.W. (2015). Glial fibrillary acidic protein: from intermediate filament assembly and gliosis to neurobiomarker. Trends Neurosci. *38*, 364–374.
24. Shalom-Feuerstein, R., Lena, A.M., Zhou, H., De La Forest Divonne, S., Van Bokhoven, H., Candi, E., Melino, G., and Aberdam, D. (2011). DeltaNp63 is an ectodermal gatekeeper of epidermal morphogenesis. Cell Death Differ. *18*, 887–896.
25. Taleahmad, S., Mirzaei, M., Parker, L.M., Hassani, S.N., Mollamohammadi, S., Sharifi-Zarchi, A., Haynes, P.A., Baharvand, H., and Salekdeh, G.H. (2015). Proteome analysis of ground state pluripotency. Sci. Rep. *5*, 17985.
26. Fu, X., Wu, S., Li, B., Xu, Y., and Liu, J. (2020). Functions of p53 in pluripotent stem cells. Protein Cell *11*, 71–78.
27. Ren, Z., Zhong, H., Song, C., Deng, C., Hsieh, H.T., Liu, W., and Chen, G. (2020). Insulin promotes mitochondrial respiration and survival through PI3K/AKT/GSK3 pathway in human embryonic stem cells. Stem Cell Rep. *15*, 1362–1376.
28. Martinez-Val, A., Lynch, C.J., Calvo, I., Ximénez-Embún, P., Garcia, F., Zarzuela, E., Serrano, M., and Munoz, J. (2021). Dissection of two routes to naive pluripotency using different kinase inhibitors. Nat. Commun. *12*, 1863.
29. Seifert, A., Werheid, D.F., Knapp, S.M., and Tobiasch, E. (2015). Role of Hox genes in stem cell differentiation. World J. Stem Cells *7*, 583–595.
30. Narendra, V., Rocha, P.P., An, D., Raviram, R., Skok, J.A., Mazzoni, E.O., and Reinberg, D. (2015). CTCF establishes discrete functional chromatin domains at the Hox clusters during differentiation. Science *347*, 1017–1021.
31. Ying, Q.L., Nichols, J., Chambers, I., and Smith, A. (2003). BMP induction of Id proteins suppresses differentiation and sustains embryonic stem cell self-renewal in collaboration with STAT3. Cell *115*, 281–292.
32. Theunissen, T.W., Powell, B.E., Wang, H., Mitalipova, M., Faddah, D.A., Reddy, J., Fan, Z.P., Maetzel, D., Ganz, K., Shi, L., et al. (2014). Systematic identification of culture conditions for induction and maintenance of naive human pluripotency. Cell Stem Cell *15*, 524–526.
33. Young, R.A. (2011). Control of the embryonic stem cell state. Cell *144*, 940–954.
34. Bhutani, K., Nazor, K.L., Williams, R., Tran, H., Dai, H., Džakula, Ž., Cho, E.H., Pang, A.W.C., Rao, M., Cao, H., et al. (2016). Whole-genome mutational burden analysis of three pluripotency induction methods. Nat. Commun. *7*, 10536.
35. Gore, A., Li, Z., Fung, H.L., Young, J.E., Agarwal, S., Antosiewicz-Bourget, J., Canto, I., Giorgetti, A., Israel, M.A., Kiskinis, E., et al. (2011). Somatic coding mutations in human induced pluripotent stem cells. Nature *471*, 63–67.
36. Williams, T.M., Leeth, R.A., Rothschild, D.E., Coutermarsh-Ott, S.L., McDaniel, D.K., Simmons, A.E., Heid, B., Cecere, T.E., and Allen, I.C.

(2015). The NLRP1 inflammasome attenuates colitis and colitis-associated tumorigenesis. J. Immunol. *194*, 3369–3380.

37. Tan, Y.Y., Zhang, Y., Li, B., Ou, Y.W., Xie, S.J., Chen, P.P., Mei, S.Q., Huang, Q.J., Zheng, L.L., and Qu, L.H. (2021). PERK signaling controls myoblast differentiation by regulating MicroRNA networks. Front. Cell Dev. Biol. *9*, 670435.
38. Hiura, H., Toyoda, M., Okae, H., Sakurai, M., Miyauchi, N., Sato, A., Kiyokawa, N., Okita, H., Miyagawa, Y., Akutsu, H., et al. (2013). Stability of genomic imprinting in human induced pluripotent stem cells. BMC Genet. *14*, 32.
39. Pei, Y., Yue, L., Zhang, W., Xiang, J., Ma, Z., and Han, J. (2018). Murine pluripotent stem cells that escape differentiation inside teratomas maintain pluripotency. PeerJ *6*, e4177.
40. Posfai, E., Schell, J.P., Janiszewski, A., Rovic, I., Murray, A., Bradshaw, B., Yamakawa, T., Pardon, T., El Bakkali, M., Talon, I., et al. (2021). Evaluating totipotency using criteria of increasing stringency. Nat. Cell Biol. *23*, 49–60.
41. Pesce, M., and Schöler, H.R. (2001). Oct-4: gatekeeper in the beginnings of mammalian development. Stem Cell. *19*, 271–278.
42. Palmieri, S.L., Peter, W., Hess, H., and Schöler, H.R. (1994). Oct-4 transcription factor is differentially expressed in the mouse embryo during establishment of the first two extraembryonic cell lineages involved in implantation. Dev. Biol. *166*, 259–267.
43. Reim, G., and Brand, M. (2002). Spiel-ohne-grenzen/pou2 mediates regional competence to respond to Fgf8 during zebrafish early neural development. Development *129*, 917–933.
44. Hochedlinger, K., Yamada, Y., Beard, C., and Jaenisch, R. (2005). Ectopic expression of Oct-4 blocks progenitor-cell differentiation and causes dysplasia in epithelial tissues. Cell *121*, 465–477.
45. Niwa, H., Miyazaki, J., and Smith, A.G. (2000). Quantitative expression of Oct-3/4 defines differentiation, dedifferentiation or self-renewal of ES cells. Nat. Genet. *24*, 372–376.
46. Stuart, H.T., Stirparo, G.G., Lohoff, T., Bates, L.E., Kinoshita, M., Lim, C.Y., Sousa, E.J., Maskalenka, K., Radzisheuskaya, A., Malcolm, A.A., et al. (2019). Distinct molecular trajectories converge to induce naive pluripotency. Cell Stem Cell *25*, 388–406.e8.
47. Wang, H., Zhao, S., Barton, M., Rosengart, T., and Cooney, A.J. (2018). Reciprocity of action of increasing Oct4 and repressing p53 in transdifferentiation of mouse embryonic fibroblasts into cardiac myocytes. Cell. Reprogram. *20*, 27–37.
48. Lee, J., Rhee, B.K., Bae, G.Y., Han, Y.M., and Kim, J. (2005). Stimulation of Oct-4 activity by Ewing's sarcoma protein. Stem Cell. *23*, 738–751.
49. Gidekel, S., Pizov, G., Bergman, Y., and Pikarsky, E. (2003). Oct-3/4 is a dose-dependent oncogenic fate determinant. Cancer Cell *4*, 361–370.
50. Beltran, A.S., Rivenbark, A.G., Richardson, B.T., Yuan, X., Quian, H., Hunt, J.P., Zimmerman, E., Graves, L.M., and Blancafort, P. (2011). Generation of tumor-initiating cells by exogenous delivery of OCT4 transcription factor. Breast Cancer Res. *13*, R94.
51. Monk, M., and Holding, C. (2001). Human embryonic genes re-expressed in cancer cells. Oncogene *20*, 8085–8091.
52. Mallo, M. (2018). Reassessing the role of Hox genes during vertebrate development and evolution. Trends Genet. *34*, 209–217.
53. Zhang, J., Yao, T., Lin, Z., and Gao, Y. (2017). Aberrant methylation of MEG3 functions as a potential plasma-based biomarker for cervical cancer. Sci. Rep. *7*, 6271.
54. Dong, Z., Zhang, A., Liu, S., Lu, F., Guo, Y., Zhang, G., Xu, F., Shi, Y., Shen, S., Liang, J., and Guo, W. (2017). Aberrant methylation-mediated silencing of lncRNA MEG3 functions as a ceRNA in esophageal cancer. Mol. Cancer Res. *15*, 800–810.
55. Yu, W., Shi, Q., Wu, C., Shen, X., Chen, L., and Xu, J. (2020). Promoter hypermethylation in fl uences the suppressive role of long non-coding RNA MEG3 in the development of multiple myeloma. Exp. Ther. Med. *20*, 637–645.
56. Miura, K., Obama, M., Yun, K., Masuzaki, H., Ikeda, Y., Yoshimura, S., Akashi, T., Niikawa, N., Ishimaru, T., and Jinno, Y. (1999). Methylation imprinting of H19 and SNRPN genes in human benign ovarian teratomas. Am. J. Hum. Genet. *65*, 1359–1367.
57. Hashimoto, K., Azuma, C., Kamiura, S., Koyama, M., Nobunaga, T., Tokugawa, Y., Kimura, T., Kubota, Y., Sawai, K., and Saji, F. (1996). Maintenance of imprinting of the insulin-like growth factor II gene (IGF2) and the small nuclear ribonucleoprotein polypeptide N gene (SNRPN) in the human uterus and leiomyoma. Gynecol. Obstet. Invest. *41*, 50–54.
58. Xu, F., Deng, C., Ren, Z., Sun, L., Meng, Y., Liu, W., Wan, J., and Chen, G. (2021). Lysophosphatidic acid shifts metabolic and transcriptional landscapes to induce a distinct cellular state in human pluripotent stem cells. Cell Rep. *37*, 110063.
59. Huang, J., Wang, F., Okuka, M., Liu, N., Ji, G., Ye, X., Zuo, B., Li, M., Liang, P., Ge, W.W., et al. (2011). Association of telomere length with authentic pluripotency of ES/iPS cells. Cell Res. *21*, 779–792.
60. Ficz, G., Branco, M.R., Seisenberger, S., Santos, F., Krueger, F., Hore, T.A., Marques, C.J., Andrews, S., and Reik, W. (2011). Dynamic regulation of 5-hydroxymethylcytosine in mouse ES cells and during differentiation. Nature *473*, 398–402.
61. Cawthon, R.M. (2002). Telomere measurement by quantitative PCR. Nucleic Acids Res. *30*, e47.
62. Liu, L., Bailey, S.M., Okuka, M., Muñoz, P., Li, C., Zhou, L., Wu, C., Czerwiec, E., Sandler, L., Seyfang, A., et al. (2007). Telomere lengthening early in development. Nat. Cell Biol. *9*, 1436–1441.
63. Poon, S.S., Martens, U.M., Ward, R.K., and Lansdorp, P.M. (1999). Telomere length measurements using digital fluorescence microscopy. Cytometry *36*, 267–278.
64. Herrera, E., Samper, E., Martín-Caballero, J., Flores, J.M., Lee, H.W., and Blasco, M.A. (1999). Disease states associated with telomerase deficiency appear earlier in mice with short telomeres. EMBO J. *18*, 2950–2960.
65. Bailey, S.M., Brenneman, M.A., and Goodwin, E.H. (2004). Frequent recombination in telomeric DNA may extend the proliferative life of telomerase-negative cells. Nucleic Acids Res. *32*, 3743–3751.
66. Dolzhenko, E., and Smith, A.D. (2014). Using beta-binomial regression for high-precision differential methylation analysis in multifactor whole-genome bisulfite sequencing experiments. BMC Bioinf. *15*, 215.
67. Love, M.I., Huber, W., and Anders, S. (2014). Moderated estimation of fold change and dispersion for RNA-seq data with DESeq2. Genome Biol. *15*, 550.
68. Yu, H.V., Tao, L., Llamas, J., Wang, X., Nguyen, J.D., Trecek, T., and Segil, N. (2021). POU4F3 pioneer activity enables ATOH1 to drive diverse mechanoreceptor differentiation through a feed-forward epigenetic mechanism. Proc. Natl. Acad. Sci. USA *118*, e2105137118.
69. Picelli, S., Björklund, A.K., Reinius, B., Sagasser, S., Winberg, G., and Sandberg, R. (2014). Tn5 transposase and tagmentation procedures for massively scaled sequencing projects. Genome Res. *24*, 2033–2040.
70. Buenrostro, J.D., Giresi, P.G., Zaba, L.C., Chang, H.Y., and Greenleaf, W.J. (2013). Transposition of native chromatin for fast and sensitive epigenomic profiling of open chromatin, DNA-binding proteins and nucleosome position. Nat. Methods *10*, 1213–1218.
71. Li, H., and Durbin, R. (2009). Fast and accurate short read alignment with Burrows-Wheeler transform. Bioinformatics *25*, 1754–1760.
72. Li, H., Handsaker, B., Wysoker, A., Fennell, T., Ruan, J., Homer, N., Marth, G., Abecasis, G., and Durbin, R.; 1000 Genome Project Data Processing Subgroup (2009). The sequence alignment/map format and SAMtools. Bioinformatics *25*, 2078–2079.
73. Liu, T. (2014). Use model-based Analysis of ChIP-Seq (MACS) to analyze short reads generated by sequencing protein-DNA interactions in embryonic stem cells. Methods Mol. Biol. *1150*, 81–95.
74. Liao, Y., Smyth, G.K., and Shi, W. (2014). featureCounts: an efficient general purpose program for assigning sequence reads to genomic features. Bioinformatics *30*, 923–930.

75. Wang, L., Feng, Z., Wang, X., Wang, X., and Zhang, X. (2010). DEGseq: an R package for identifying differentially expressed genes from RNA-seq data. Bioinformatics *26*, 136–138.

76. Ramírez, F., Dündar, F., Diehl, S., Grüning, B.A., and Manke, T. (2014). deepTools: a flexible platform for exploring deep-sequencing data. Nucleic Acids Res. *42*, W187–W191.

77. Wang, K., Li, M., and Hakonarson, H. (2010). ANNOVAR: functional annotation of genetic variants from high-throughput sequencing data. Nucleic Acids Res. *38*, e164.

78. Sherry, S.T., Ward, M.H., Kholodov, M., Baker, J., Phan, L., Smigielski, E.M., and Sirotkin, K. (2001). dbSNP: the NCBI database of genetic variation. Nucleic Acids Res. *29*, 308–311.

79. Cibulskis, K., Lawrence, M.S., Carter, S.L., Sivachenko, A., Jaffe, D., Sougnez, C., Gabriel, S., Meyerson, M., Lander, E.S., and Getz, G. (2013). Sensitive detection of somatic point mutations in impure and heterogeneous cancer samples. Nat. Biotechnol. *31*, 213–219.

80. Saunders, C.T., Wong, W.S.W., Swamy, S., Becq, J., Murray, L.J., and Cheetham, R.K. (2012). Strelka: accurate somatic small-variant calling from sequenced tumor-normal sample pairs. Bioinformatics *28*, 1811–1817.

81. Boeva, V., Popova, T., Bleakley, K., Chiche, P., Cappo, J., Schleiermacher, G., Janoueix-Lerosey, I., Delattre, O., and Barillot, E. (2012). Control-FREEC: a tool for assessing copy number and allelic content using next-generation sequencing data. Bioinformatics *28*, 423–425.

82. Talevich, E., Shain, A.H., Botton, T., and Bastian, B.C. (2016). CNVkit: genome-wide copy number detection and visualization from targeted DNA sequencing. PLoS Comput. Biol. *12*, e1004873.

83. Krueger, F., and Andrews, S.R. (2011). Bismark: a flexible aligner and methylation caller for Bisulfite-Seq applications. Bioinformatics *27*, 1571–1572.

84. Wang, L., Zhang, J., Duan, J., Gao, X., Zhu, W., Lu, X., Yang, L., Zhang, J., Li, G., Ci, W., et al. (2014). Programming and inheritance of parental DNA methylomes in mammals. Cell *157*, 979–991.

85. Robinson, J.T., Thorvaldsdóttir, H., Winckler, W., Guttman, M., Lander, E.S., Getz, G., and Mesirov, J.P. (2011). Integrative genomics viewer. Nat. Biotechnol. *29*, 24–26.

STAR★METHODS

KEY RESOURCES TABLE

REAGENT or RESOURCE	SOURCE	IDENTIFIER
Antibodies		
Oct4	Santa Cruz	Cat#: sc5279; RRID: AB_628051
Nanog	Abcam	Cat#: ab80892; RRID: AB_2150114
Lin28a	CST	Cat#: 3978S; RRID: AB_2297060
SSEA1	Millipore	Cat#: MAB4301; RRID: AB_177627
Zscan4	Millipore	Cat#: AB4340; RRID: AB_2827621
MuERVL-Gag	EpiGentek	Cat#: A-2801-100; Uniprot: V9H130
Dnmt3a	Abcam	Cat#: ab2850; RRID: AB_303355
Dnmt3b	Abcam	Cat#: ab13604; RRID: AB_300494
Dnmt3l	CST	Cat#: 13451S; RRID: AB_2798222
ERK1/2	CST	Cat#: 9102S; RRID: AB_330744
Phospho-ERK1/2	CST	Cat#: 9106S; RRID: AB_331768
β-Actin	Abmart	Cat#: P30002; RRID: AB_2222847
5-methylcytosine (5mC)	Millipore	Cat#: NA81; RRID: AB_213180
5-hydroxymethylcytosine (5hmC)	active-Motif	Cat#: 39769; RRID: AB_10013602
βIII-tubulin	Chemicon	Cat#: CBL412; RRID: AB_11211667
α-SMA	Abcam	Cat#: ab5694; RRID: AB_2223021
AFP	Dako	Cat#: DAK-N1501
Nestin	Millipore	Cat#: MAB353; RRID: AB_94911
GFAP	Abcam	Cat#: ab33922; RRID: AB_732571
P63	Abcam	Cat#: ab124762; RRID: AB_10971840
Sox2	Abcam	Cat#: ab92494; RRID: AB_10585428
Alexa Fluor® 594 Goat Anti-Rabbit IgG (H + L)	Jackson	Cat#: 111-585-003; RRID: AB_2338059
Alexa Fluor® 488 Goat Anti-Rabbit IgG (H + L)	Life	Cat#: A11008; RRID: AB_143165
Alexa Fluor® 594 Goat Anti-Mouse IgG (H + L)	Life	Cat#: A11005; RRID: AB_141372

(*Continued on next page*)

Continued

REAGENT or RESOURCE	SOURCE	IDENTIFIER
Alexa Fluor® 594 Donkey Anti-Goat IgG (H + L)	Abcam	Cat#: ab150132; RRID: AB_2810222
Donkey anti-Rabbit IgG-HRP	GE Healthcare	Cat#: NA934V; RRID: AB_772206
Goat anti-Mouse IgG (H + L)/HRP	ZSGB-BIO	Cat#: ZB2305; RRID: AB_2747415
Chemicals, peptides, and recombinant proteins		
ESGRO (mLIF)	Millipore	Cat#: ESG1107
PD0325901	Miltenyi	Cat#: 04-0006
CHIR99021	Selleck	Cat#: S1263
Recombinat human LIF	Millipore	Cat#: LIF1010
CGP77675	Cayman	Cat#: 21089
(S)-(+)-Dimethindene maleate (Dim)	Tocris	Cat#: 1425
Minocycline hydrochloride (Mih)	Tocris	Cat#: 3268
Nocodazole	Sigma	Cat#: M1404
Critical commercial assays		
RNeasy Plus Mini Kit	Qiagen	Cat#: 74134
DNeasy Blood & Tissue Kit	Qiagen	Cat#: 69504
QIAquick Gel Extraction Kit	Qiagen	Cat#: 28704
pEASY-T1 Simple Cloning Kit	Transgene	Cat#: CT111
TeloChaser Telomerase assay kit	MD Biotechnology	Cat#: T0001
Mouse Telomerase (TE) ELISA kit	CUSABIO	Cat#: CSB-E08022
TruSeq PE Cluster Kit	Illumina	Cat#: PE-201-5001
TruePrep DNA Library Prep Kit V2 for Illumina®	Vazyme Biotech	Cat#: TD503-02
Deposited data		
RNA sequencing data	This paper	GSE157876
ATAC sequencing data	This paper	GSE157876
Exome sequencing data	This paper	GSE157876
RRBS data	This paper	GSE213109
Experimental models: Cell lines		
mESCs	This paper	N/A
Experimental models: Organisms/strains		
C57BL/6 mice	Beijing Vital River Laboratory Animal Technology Co., Ltd.	213
129 mice	Beijing Vital River Laboratory Animal Technology Co., Ltd.	217
C3H mice	Beijing Vital River Laboratory Animal Technology Co., Ltd.	212
ICR mice	Beijing Vital River Laboratory Animal Technology Co., Ltd.	201
Kunming (KM) mice	Beijing Vital River Laboratory Animal Technology Co., Ltd.	202
Software and algorithms		
GraphPad Prism software	GraphPad Software	https://www.graphpad.com
TFL-TELO program	Kindly provided by Peter Lansdorp, Terry Fox Laboratory	N/A
RStudio	RStudio	https://posit.co/downloads/
R package of "pheatmap," "cor" and "ggplot2"	Bioconductor	https://bioconductor.org; https://ggplot2.tidyverse.org

(*Continued on next page*)

Continued

REAGENT or RESOURCE	SOURCE	IDENTIFIER
Integrative Genomics Viewer	Broad Institute	https://software.broadinstitute.org/software/igv/
StatView software	SAS Institute Inc.	https://statview.software.informer.com

RESOURCE AVAILABILITY

Lead contact

Further information and requests for resources and reagents should be directed to and will be fulfilled by the lead contact, Lin Liu (liulin@nankai.edu.cn).

Materials availability

All unique/stable reagents and the ES cell lines generated in this study are available from the lead contact with a completed Materials Transfer Agreement.

Data and code availability

- RNA-seq, ATAC-seq, Exome-seq, RRBS datasets (raw files and processed count matrices) collected in this study have been deposited at GEO under the accession number provided in the key resources table. Accession numbers are listed in the key resources table. Original western blot images and microscopy data reported in this paper will be shared by the lead contact upon request.
- This paper does not report the original code. This study uses referenced sources of code that can be found in the vignettes of the cited packages. Details of the packages are provided in the key resources table, and the parameters are provided in the method details section.
- Any additional information required to reanalyze the data reported in this paper is available from the lead contact upon request.

EXPERIMENTAL MODEL AND STUDY PARTICIPANT DETAILS

Mouse ESC

mESC lines were established, characterized, and maintained based on the method described,[59] basically following the original methods.[12] Blastocysts were isolated from the uterine horns of pregnant females at Embryo (E) day 3.5 using a dissection microscope in HKSOM and plated onto mitomycin C-treated MEF cells (from B6C3F1 mice E13.5 embryos) served as feeders in KSR/DMEM added with PD0325901 and LIF (K/DL) medium and cultured for 7 days to form outgrowths. Emerging ICM outgrowths were directly picked into serum/LIF (S/L) medium on feeders to establish stable mESC lines. Established mESC lines were genotyped by *Sry* gene to determine the sex. All the mESC used in this study are male (XY). mESC lines were maintained by dissociating cells with 0.25% TE (Invitrogen) every 2–3 days and re-plated onto feeder cells. K/DL medium contains knockout DMEM (Invitrogen) supplemented with 20% Knockout serum replacement (KSR, Invitrogen), 1 mM L-glutamine, 1% nonessential amino acid stock, 50 units/ml penicillin and 50 μg/mL streptomycin (2A, Invitrogen), 0.1 mM β-mercaptoethanol (Invitrogen), 1 μM PD0325901 and 1000 IU/mL mouse LIF (mLIF, Millipore). S/L medium (ESC culture medium) contains knockout DMEM supplemented with 15% FBS (ES quality, Hyclone), 1 mM L-glutamine, 1% nonessential amino acid stock, 50 units/ml penicillin and 50 μg/mL streptomycin, 0.1 mM β-mercaptoethanol, and 1000 IU/mL mLIF. ESCs were cultured at 37°C in 5% CO_2 incubator with humidified air.

After culture mESCs in S/L for 4 passages, mESCs were derived and maintained by dissociating cells with 0.25% TE every 2–3 days and re-plating them onto feeder cells (for S/L, 2iL, a2iL and LCDM) or Poly-L-lysine hydrobromide/Laminin A coated wells. For 2iL and 2iL-F culture system: 1:1 mixture of DMEM/F12 supplemented with N2 (Invitrogen) and Neurobasal media with glutamine (Invitrogen) supplemented with B27 (Invitrogen), 1 mM L-glutamine, 1% nonessential amino acid stock, 50 units/ml penicillin and 50 μg/mL streptomycin, 0.1 mM β-mercaptoethanol, and 1000 IU/mL mLIF, 1 μM PD0325901 and 3 μM CHIR99021 (Selleck). For a2iL culture system: 1:1 mixture of DMEM/F12 supplemented with N2 and Neurobasal media with glutamine supplemented with B27, 1 mM L-glutamine, 1% nonessential amino acid stock, 50 units/ml penicillin and 50 μg/mL streptomycin, 0.1 mM β-mercaptoethanol, and 1000 IU/mL mLIF, 3 μM CHIR99021 and 1.5 μM CGP77675 (Cayman). For LCDM culture system: 1:1 mixture of DMEM/F12 supplemented with N2 and Neurobasal media with glutamine supplemented with B27, 5% KSR, 1 mM L-glutamine, 1% nonessential amino acid stock, 50 units/ml penicillin and 50 μg/mL streptomycin, 0.1 mM β-mercaptoethanol, and 1000 IU/mL mLIF, 3 μM CHIR99021, 2 μM (S)-(+)-Dimethindene maleate (Dim, Tocris) and 2 μM Minocycline hydrochloride (Mih, Tocris).

Mice

Use of mice for this research was approved by the Nankai University Animal Care and Use Committee (License number 20140006). All mice used in this study were taken care of and operated according to the relevant regulations. Mice were housed and cared in individually ventilated cages (IVCs) on a standard 12 h light: 12 h dark cycle in the sterile Animal Facility at College of Life Sciences. 6-8-week-old C57BL/6 (female), 8-week-old C3H (male), 8-week-old 129 (male), 6-8-week-old ICR (female) and 6-8-week-old Kunming (KM, female) mice were obtained from Beijing Vital River Laboratory Animal Technology Co., Ltd. The ESC-mice (male) are derived from mESC by tetraploid embryo complementation (TEC) assay.

METHOD DETAILS

Tetraploid embryo complementation (TEC) assay

Tetraploid (4 N) embryos were produced by the electrofusion of two-cell stage embryos collected from albino strain ICR mice. Two-cell embryos were induced to fuse by two pulses of 1,200 V/cm DC for 50 μs, after an AC pulse of 75 V/cm for 5 s, generated from an Eppendorf Multiporator. About 10–15 ESCs were injected into one tetraploid blastocyst and the injected blastocysts were transferred into surrogate Kunming females to produce ESC-mice. Genotyping of ESC- mice was confirmed by standard DNA microsatellite genotyping analysis using D12Mit136 (5′-TTTAATTTTGAGTGGGTTTGGC-3′ and 5′-TTGCTACATGTACACTGATCTCCA-3′) and D8Mit4 (5′-GGCTGCAATGCGGTTCCGTAGA-3′ and 5′-TGAAGAGGACGCTTTGGATGAT-3′) primers. ESC- mice were mated with albino strain ICR mice to further examine their germline transmission competence.

Tissue collection and histology

Tumors were collected from ESC- mice when they were 18–24 months old and stored frozen at −80°C in a freezer. The stored tissues were thawed, washed with PBS for 10 min, and fixed in 3.7% paraformaldehyde (PFA) overnight at 4°C. The tissue was washed three times and dehydrated with different concentrations of ethanol in sequence for 1 h each time. Then xylene was added for clear treatment twice about 30 min each time. Afterward, the cleared tissue was marked and immersed in wax three times, with the concentration of wax gradually increased three times 1 h each time. An automatic paraffin tissue embedding machine was used for tissue embedding, and the embedded paraffin block was stored at 4°C. Sections were cut in 5 μm, dried at 65°C and stored at room temperature. After deparaffinization with xylene and rehydration with different concentrations of ethanol, sections were stained with hematoxylin and eosin Y (H&E) for an appropriate time. Sections were washed and treated with different concentrations of ethanol and xylene, neutral resin was added to seal the slides and stored. Images were collected by CCD camera using LMD6000 (for the whole tumor images) or Leica DFC420C (for high-magnification images). The laser microdissection system LMD6000 was used to take several images in the setting area and automatically combine these areas for the whole tumor image.

Immunofluorescence microscopy

For immunofluorescence of tissue sections, following deparaffinization, rehydration, sections were boiled for 3 min at 120°C in 0.01% sodium citrate buffer (pH = 6.0) for antigen retrieval, permeabilized in 0.2% Triton X-100 in PBS for 30 min, blocked with 3% goat serum and 0.1% BSA for 2 h, then incubated with primary antibodies (anti-SMA, anti-Nestin, anti-GFAP, anti-βIII-Tubulin, anti-P63, anti-AFP, anti-Oct4, anti-Nanog, or anti-Sox2) at 4°C overnight. After washing with PBS three times, sections were incubated with an appropriate secondary antibody (Alexa Fluor 594 or 488) for 2 h at room temperature. After washing, the slides were mounted in Vectashield (Vector Laboratories) containing 1 μg/mL Hoechst 33342.

As to immunofluorescence of cells, cells were washed twice in PBS, fixed in freshly prepared 3.7% PFA fixation for 30 min on ice, washed once in PBS and permeabilized in 0.1% Triton X-100 in blocking solution (3% goat serum plus 0.1% BSA in PBS) for 30 min at room temperature, blocked for 2 h and then incubated with primary antibodies (anti-Oct4, anti-Nanog, anti-SSEA1, anti-Zscan4, anti-MuERVL-Gag, anti-Sox2, anti-Nestin, anti-GFAP, or anti-P63) at 4°C overnight. After washing with PBS three times, cells were incubated with an appropriate secondary antibody (Alexa Fluor 594 or 488) for 2 h at room temperature. After washing, the slides were mounted in Vectashield (Vector Laboratories) containing 1 μg/mL DAPI or Hoechst. Images were captured using a Zeiss Axio Imager Z2 microscope or LSM 700 laser scanning confocal microscope (Carl Zeiss).

To detect 5hmC and 5mC, sections were washed three times for 5 min with PBS. Post-fixed sections were first permeabilized for 30 min with 0.5% Triton X-100 (in 1% BSA in PBS), and subsequently treated with RNase A (10 μg/mL) in 1% BSA in PBS for 1 h at 37°C. After three 5 min washes with PBS, sections were incubated with 4N HCl for 10 min at 37°C to denature genomic DNA and then washed three times for 10 min with PBS and permeabilized in 0.1% Triton X-100 in blocking solution (3% goat serum plus 0.1% BSA in PBS) for 30 min at room temperature, blocked for 2 h and then incubated with primary antibodies (anti-5mC and anti-5hmC) at 4°C overnight. After washing with PBS for three times, cells were incubated with appropriate secondary antibody (Alexa Fluor 594 or 488) for 2 h at room temperature. After washing, the slides were mounted in Vectashield (Vector Laboratories) containing 1 μg/mL DAPI. Images were captured using a Zeiss Axio Imager Z2 (Carl Zeiss).

Western blot

Cells were washed twice in PBS, collected, and lysed in cell lysis buffer on ice for 30 min and then sonicated for 1 min at 60 of amplitude at 2 s intervals. After centrifugation at 10,000 g at 4°C for 10 min, supernatant was transferred into new tubes. The concentration of the cell protein sample was measured by bicinchoninic acid, and protein samples boiled in SDS sample buffer at 95°C for 10 min.

The cell extract sample was resolved by 10% Acr-Bis SDS-PAGE and transferred to polyvinylidene difluoride membranes (PVDF, Millipore). Nonspecific binding was blocked by incubation in 5% nonfat milk or 5% BSA in TBST at room temperature for 2 h. Blots were then probed with primary antibodies overnight by incubation at 4°C with anti-Oct4, anti-Nanog, anti-Lin28a, anti-Dnmt3a, anti-Dnmt3b, anti-Dnmt3l, anti-ERK, or anti-phosphorylated ERK (pERK). β-Actin served as loading control. Immunoreactivity bands were then probed for 2 h at room temperature with horseradish peroxidase (HRP)-conjugated secondary antibodies (HRP-goat anti-rabbit IgG and HRP-goat anti-mouse IgG). Protein bands were detected by Chemiluminescent HRP substrate (WBKLS0500, Millipore).

Gene expression analysis by real-time qPCR

Total RNA was purified using RNA mini kit (QIAGEN), treated with DNase I (QIAGEN), and the cDNA was generated from 2 μg RNA using Oligo (dT)18 primer (Takara) and M-MLV Reverse Transcriptase (Invitrogen). Real-time quantitative PCR (qPCR) reactions were set up in duplicate with the FS Universal SYBR Green Master (Roche) and carried out on an iCycler MyiQ2 Detection System (Bio-Rad). All reactions were carried out by amplifying target genes and internal control in the same plate. Each sample was repeated three times and normalized using Gapdh as the internal control. The amplification was performed for primary denaturation at 95°C for 10 min, then 40 cycles of denaturation at 95°C for 15 s, annealing and elongation at 58°C for 1 min, and the last cycle under 55–95°C for dissociation curve. Relative quantitative evaluation of target gene was determined by comparing the threshold cycles. Primers (Gapdh: 5′-TCAACAGCAACTCCCACTCTTCCA-3′ and 5′-ACCACCCTGTTGCTGTAGCCGTAT-3′; Dnmt3a: 5′-CAGCAC CATTCCTGGTCATGCAAA-3′ and 5′-TCCTGTGTGGTAGGCACCTGAAA-3′; Dnmt3b: 5′-CGGAAAGCAACCCAAAGCAATAC-3′ and 5′-CCTCGGAACCATAGGAAACATTC-3′) were confirmed for their specificity with dissociation curves.

Dot blot

Total 5mC and 5hmC levels were measured by dot blot analysis based on the method described previously.[60] Briefly, genomic DNA was isolated by DNeasy Blood & Tissue Kit (Qiagen, Valencia, CA) and denatured in 0.4 N NaOH and 10 mM EDTA at 95°C for 10 min, and 2-fold serial dilutions were spotted on positively charged nylon membranes. The membranes were immunoblotted with 5mC or 5hmC antibody, followed by HRP conjugated goat anti-mouse or anti-rabbit antibodies. DNA loading was verified by staining with methylene blue.

Telomerase activity by TRAP assay

Telomerase activity was determined by the Stretch PCR method according to manufacturer's instruction using TeloChaser Telomerase assay kit (T0001, MD Biotechnology). About 2×10^4 cells from each sample were lysed. Lysis buffer served as negative control. PCR products of cell lysate were separated on non-denaturing TBE-based 12% polyacrylamide gel electrophoresis and visualized by ethidium bromide (EB) staining.

Telomerase assay by ELISA

Telomerase level was determined by ELISA method according to manufacturer's instruction using Mouse Telomerase (TE) ELISA kit (CSB-E08022m, CUSABIO).

Telomere measurement by real-time qPCR

Genome DNA was prepared using DNeasy Blood & Tissue Kit (Qiagen, Valencia, CA). Average telomere length was measured from total genomic DNA using a real-time PCR assay.[61] PCR reactions were performed on the iCycler iQ5 2.0 Standard Edition Optical System (Bio-Rad, Hercules, CA), using telomeric primers, primers for the reference control gene (mouse 36B4 single copy gene) and PCR settings as previously described.[62] For each PCR reaction, a standard curve was made by serial dilutions of known amounts of DNA. The telomere signal was normalized to the signal from the single copy gene to generate a T/S ratio indicative of relative telomere length. Equal amount of DNA (20 ng) was used for each reaction. 36B4 primer: 5′-ACTGGTCTAGGACCCGAGAAG-3′ and 5′-TCAATGGTGCCTCTGGAGATT-3′, Telomere primer: 5′-CGGTTTGTTTGGGTTTGGGTTTGGGTTTGGGTTTGGGTT-3′ and 5′-GG CTTGCCTTACCCTTACCCTTACCCTTACCCTTACCCT-3′.

Telomere Q-FISH

Telomere length was estimated by telomere Q-FISH as described previously.[63,64] Telomeres were denatured at 80°C for 3 min and hybridized with FITC-labeled $(CCCTAA)_3$ peptide nucleic acid (PNA) probe at 0.5 μg/mL (F1009, Panagene, Korea). Chromosomes were stained with 0.5 μg/mL DAPI. Fluorescence from chromosomes and telomeres was digitally imaged on a Zeiss microscope with FITC/DAPI using AxioCam and AxioVision software 4.6. Telomere length shown as telomere fluorescence intensity was integrated using the TFL-TELO program (kindly provided by Peter Lansdorp).

Telomere chromosome orientation-fluorescence in situ hybridization (CO-FISH)

CO-FISH assay was performed as described,[65] with slight modification. mESCs were incubated with 10 μM BrdU for 12 h. 0.3 μg/mL Nocodazole at was added for 3 h prior to cell harvest, and metaphase spreads were prepared by a routine method. Chromosome slides were treated with RNaseA, fixed with 4% formaldehyde, then stained with Hoechst33258 (0.5 μg/mL), incubated

in 2 × SSC (Invitrogen) for 15 min and exposed to 365 nm UV light (Stratalinker 1800UV irradiator) for 40 min. The BrdU-substituted DNA was digested with Exonuclease III (Takara). Telomeres were denatured at 80°C for 3 min and hybridized with FITC-labeled $(CCCTAA)_3$ peptide nucleic acid (PNA) probe at 0.5 μg/mL (F1009, Panagene, Korea). Chromosomes were stained with 0.5 μg/mL DAPI. Fluorescence from chromosomes and telomeres was digitally imaged on a Zeiss microscope with FITC/DAPI using AxioCam and AxioVision software 4.6. To analyze telomere sister chromatid exchange (T-SCE), one signal at each end of the chromosome was counted as no T-SCE, while two signals at both chromatids on one chromosome end were identified as one T-SCE.

RNA-sequencing and analysis

mRNA was purified from total RNA using poly-T oligo-attached magnetic beads. Fragmentation was carried out using divalent cations under elevated temperature in NEB Next First Strand Synthesis Reaction Buffer (5x). First strand cDNA was synthesized using random hexamer primer and M-MLV Reverse Transcriptase (RNase H^-). Second strand cDNA synthesis was subsequently performed using DNA Polymerase I and RNase H. Remaining overhangs were converted into blunt ends via exonuclease/polymerase activities. After adenylation of 30 ends of DNA fragments, NEB Next Adaptors with hairpin loop structure were ligated to prepare for hybridization. To select cDNA fragments of preferentially 150–200 bp in length, the library fragments were purified with AMPure XP system (Beckman Coulter, Beverly, USA). Then 3 μL USER Enzyme (NEB, USA) was used with size-selected and cDNA adaptor ligated at 37°C for 15 min followed by 5 min at 95°C prior to PCR. PCR was performed with Phusion High-Fidelity DNA polymerase, Universal PCR primers and Index Primer. At last, PCR products were purified using AMPure XP system and library quality assessed on the Agilent Bioanalyzer 2100 system. Cluster of the index-coded samples was performed on a cBot Cluster Generation System using TruSeq PE Cluster Kit (Illumina) according to the manufacturer's instructions. After cluster generation, the library preparations were sequenced on an Illumina Hiseq platform.

For RNA-seq analysis, clean reads were mapped to the mouse reference mm10 reference genome using Hisat2. Reads were assigned and counted to genes using the Feature-counts. The resulting matrix of read counts was then loaded into RStudio (R version 3.4.2), and DESeq2 used to identify differentially expressed genes. Functional enrichment (GO annotation or KEGG) of gene sets with different expression patterns was performed using clusterProfiler. The heat-maps were drawn by the function "pheatmap" of R packages and correlation coefficients calculated by the function "cor" in R. Scatterplots were generated using the "ggplot2" package to graphically reveal genes that differ significantly between two samples. The p values were adjusted using the Benjamin & Hochberg method. Corrected p-value of 0.05 and two-fold changes were set as the threshold for significantly differential gene expression. Calculated *Z* score of selected genes was used for heatmap. For analysis of TEs, clean reads were aligned to the mm10 reference by STAR with parameters '-winAnchorMultimapNmax 100' and '-outFilterMultimapNmax 100'. TEs annotated in UCSC Genome Browser (RepeatMasker) were counted using featureCounts. The DESeq2 was subsequently applied to identify differentially expressed transposable elements, and only the transposable elements with expression fold change >1.5 and adjusted p value < 0.05 from DEseq2 results were considered to be differentially expressed.

For identification common imprinting related DEGs, DESeq2 were used to identify differentially expressed genes with adjusted p value less than 0.001.[66] Known imprinted genes list was obtained from genomic imprinting website (https://www.geneimprint.com/site/home). The imprinted genes show differential expression in all groups compared to ESC in S/L are regards as common imprinting related DEGs.

ATAC-sequencing and analysis

Cell lysis and tagmentation was based on the method,[67] with some modifications, including the elimination of the nuclear purification step. Hyperactive Tn5 was produced as previously described.[68] The transposition activity of homemade Tn5 was assessed, and activity defined as the amount of transposase that was able to convert 100 ng λDNA to fragments of an average size of 200–400 bp in 15 min at 55°C. Cells (500–3000 cells per reaction) were centrifuged to remove the supernatant. 20 μL of lysis buffer [10 mM Tris HCl (pH 7.4), 5 mM $MgCl_2$, 10% DMF, 0.2% N-P40] was added, followed by pipetting 6–10 times to release the nuclei without purification, and 30 μL reaction buffer [10 mM Tris HCl (pH 7.4), 5 mM $MgCl_2$, 10% DMF, 1000 unit Tn5] was mixed on a Vortex for 5 s. The reaction was incubated at 37°C for 20 min, followed by addition of 350 μL ERC buffer (MiniElute, Qiagen) to stop the reaction. After DNA purification (MiniElute, Qiagen), ATAC-seq libraries were constructed as previously described.[69]

All ATAC-seq reads were mapped to the mm10 genome by BWA after being trimmed by Trimmomatic.[70] All unmapped reads, non-uniquely mapped reads and PCR duplicates were removed by samtools.[71] Then ATAC-Seq peak regions of each sample were called using MACS2 with parameters –nomodel –shift −100 -B –extsize 200 -g mm -f BAMPE.[72] To generate a consensus set of unique peaks, we next merged the ATAC-Seq peaks for which the distance between proximal ends was less than one base pair. In total, we identified 73,292 peaks from all samples. For each sample, the fragments were counted across each peak region using featureCounts.[73,74] Then DEseq2 was used to identify the different chromatin accessibility peaks with p value less than 0.05. Deeptools was used for visualization.[75]

Whole-exome sequencing and analysis

Sample gDNA was extracted, and the Exon-seq database construction and sequencing work were all carried out by Beijing Novogene Company as follows. Paired-end DNA library was prepared according to manufacturer's instructions (Agilent). Genomic DNAs (gDNA) from cell samples were sheared into 180–280 bp fragments by Covaris S220 sonicator. Ends of gDNA fragments were

repaired and 30 ends were adenylated. Both ends of gDNA fragments were ligated at the 30 ends with paired-end adaptors (Illumina) with a single 'T' base overhang and purified using AMPure SPRI beads from Agencourt. The adaptor-modified gDNA fragments were enriched by six cycles of PCR using SureSelect Primer and SureSelect ILM Indexing PreCapture PCR Reverse Primer. The concentration and size distribution of the libraries were determined on an Agilent Bioanalyzer DNA 1000 chip. Whole exome capture was carried out using SureSelect Mouse All Exon V1 Agilent 5190–4642. An amount of 0.5 μg prepared gDNA library was hybridized with capture library for 5 min at 95°C followed by 24 h at 65°C. The captured DNA-RNA hybrids were recovered using Dynabeads MyOne Streptavidin T1. Capture products were eluted from the beads and desalted using QIAGEN MinElute PCR purification columns. The purified capture products were then amplified using the SureSelect ILM Indexing Post Capture Forward PCR Primer and PCR Primer Index (Agilent) for 12 cycles. After DNA quality assessment, captured DNA library was sequenced on Illumina Hiseq 2000 sequencing platform (Illumina) according to manufacturer's instructions for paired-end 150 bp reads (Novogene). Libraries were loaded onto paired-end flow cells at concentrations of 14–15 pM to generate cluster densities of 800,000–900,000 per mm^2 using Illumina cBot and HiSeq paired-end cluster kit.

For Exome-seq analysis, paired-end clean reads in FastQ format generated by the Illumina pipeline were aligned to the mouse reference genome mm10 by Burrows-Wheeler Aligner (BWA) to obtain the original mapping results stored in BAM format.[70] SAMtools were used to sort BAM files and generate final BAM files for computation of the sequence coverage and depth.[71] For ESCs samples, BCF tools were used to call variants, and variants annotation and variant positions were obtained using ANNOVAR.[76] Variants obtained from previous steps were compared against variants present in the dbSNP database using SnpSift to discard background variants.[77] For tumor samples, the consensus sequences were then used to compare with blood samples from the same genetic background mice to examine candidate novel mutations in coding sequence (CDS). The muTect was used to call SNV (Single nucleotide variants), and Strelka to call Indel (insertion - deletion).[78,79]

The CNV (Copy Number Variation) which contained the deletion and duplication was determined by the software Control-FREEC.[80] Mouse Embryonic Fibroblast (MEF) or tail-tip fibroblasts (TTF) at the same genetic background served as reference control for analysis of CNVs in ESC samples. Blood samples from the same genetic background mice served as reference control for analysis of the tumor samples. Because ESCs under conventional cultures produced ESC-mice that showed no visible abnormalities, they served as the reference control to further examine whether the mutations and CNVs were shared between other ESCs and tumors, based on the methods described previously.[34,35] CNVkit was used for CNV analysis and drawing heatmap.[81]

Genome-wide DNA methylation analysis by RRBS

For Reduced Representation Bisulfite Sequencing (RRBS) data processing, clean reads were mapped to the mouse genome (mm10) using Bismark (version 0.17.0).[82] Mapped reads were further deduplicated and filtered for non-conversion. Estimation of methylation levels were determined in the CpG context with Bismark. By using the normal muscle as the control, the differently methylated regions (DMRs) were identified in teratomas by RADMeth,[83] with adjusted p values less than 0.05. DMRs sites less than 200 bp away were then merged into DMR candidates. We ultimately selected candidates that contained more than three differently methylated CGs (among which the mean-meth-diff was greater than 0.2) as differently methylated regions.

RefSeq gene annotation (mm10) was download from the UCSC website, and promoters are defined as regions 2 kb upstream from TSSs (transcriptional start sites) for each RefGene transcript.[84] The methylation level was estimated as the number of reads showing methylation over position/total reads (methylated and unmethylated).[84] For data visualization, bigwig files were generated using bedGraphToBigWig from the UCSC website and visualized in the Integrative Genomics Viewer (IGV, version 2.7.2).[85]

QUANTIFICATION AND STATISTICAL ANALYSIS

Statistics was analyzed by using the StatView software from SAS Institute Inc. (Cary, NC). Data were analyzed using two-tailed unpaired Student's t test to compare two groups or ANOVA to compare more than two groups and expressed as Mean ± SEM or Mean ± SD. p values less than 0.05 were considered significant (*$p < 0.05$, **$p < 0.01$ or ***$p < 0.001$). Fisher's exact test was used to determine if the proportions of categories in two group variables significantly differ from each other. The exact values of "n" used are described in the corresponding figure legends. "n" refers to the number of biological replicates and includes either number of mice or replicates of cell studies. Graphs were generated using GraphPad Prism or R package ggplot2 or other R packages.